

Effective Vs and Vp characterization from Surface Waves streamer data along river embankments

Original

Effective Vs and Vp characterization from Surface Waves streamer data along river embankments / Comina, C.; Vagnon, F.; Arato, A.; Antonietti, A.. - In: JOURNAL OF APPLIED GEOPHYSICS. - ISSN 0926-9851. - 183:(2020), pp. 104221-104232. [10.1016/j.jappgeo.2020.104221]

Availability:

This version is available at: 11583/2959420 since: 2022-03-24T20:34:23Z

Publisher:

Elsevier

Published

DOI:10.1016/j.jappgeo.2020.104221

Terms of use:

This article is made available under terms and conditions as specified in the corresponding bibliographic description in the repository

Publisher copyright

Elsevier postprint/Author's Accepted Manuscript

© 2020. This manuscript version is made available under the CC-BY-NC-ND 4.0 license
<http://creativecommons.org/licenses/by-nc-nd/4.0/>. The final authenticated version is available online at:
<http://dx.doi.org/10.1016/j.jappgeo.2020.104221>

(Article begins on next page)

Journal of Applied Geophysics

Effective Vs and Vp characterization from Surface Waves streamer data along river embankments. --Manuscript Draft--

Manuscript Number:	APPGEO_2020_363R1
Article Type:	Research Paper
Section/Category:	Near-surface, Engineering seismics, Ground-penetrating radar
Keywords:	river embankments.; surface waves; seismic characterization
Corresponding Author:	Cesare Comina DST - Università di Torino Torino, Italy
First Author:	Cesare Comina
Order of Authors:	Cesare Comina Federico Vagnon Alessandro Arato Andrea Antonietti
Abstract:	<p>River embankments are linearly extended earth structures built for river flood protection. Their continuity and uniformity are fundamental prerequisites to ensure and maintain their protection efficiency. Weakness points usually develop in localized areas where geotechnical variability is present in the embankment body or in the underlying subsoil. Given their significant length, and the localized nature of weakness points, the characterization of river embankments cannot therefore rely on local geotechnical investigations but requires the application of efficient and economically affordable methods, able to investigate relevant lengths in a profitable way. This is even more essential when the investigations are conducted near, or in foresee of, significant flood events, when timing of the surveys is essential. In this paper the application of a procedure (W/D procedure) for the seismic characterization of river embankments, specifically designed for surface waves streamer data, is presented. The W/D procedure allows the combined definition of 2D shear (Vs) and compressional (Vp) wave velocity models and can be developed in order to be automated as a fast imaging tool. Its application to the characterization of a test site (Bormida river embankment, Piedmont Region, Italy) is presented. It is also shown that the obtained results are comparable to standard seismic processing approaches with the advantage of reduced survey time and increased efficiency, giving preliminary results directly in the field.</p>
Suggested Reviewers:	John Lane jwlane@usgs.gov Referenced for the use of MASW testing over embankments. Lutz Karl lkarl@geotomographie.de Expert in MASW testing for embankment characterization.
Opposed Reviewers:	
Response to Reviewers:	

Dear Editor and Reviewers,

we would like to thank you very much for your revision of our paper. We improved (in our opinion) the previous submitted manuscript according to your comments and suggestions.

The main point raised by both reviewers was related to the need for more explanations with respect to the adopted W/D procedure and the way in which through this procedure also the Vp information can be extracted. We have done some more effort in this respect in order to better explain the main crucial points of the W/D procedure for the presented application.

Nevertheless, we have not excessively extended the explanations since the W/D procedure is clearly explained in several already published papers, all referenced. Therefore, a too detailed explanation would be only a duplication of the current available literature. We hope the reviewers will be satisfied with the proposed revisions and with the added explanations given.

We attached two versions of the revised manuscript: a cleaned copy and a copy with underlined revisions in order to directly visualize where in the paper we have done our modifications.

Hereafter, we also provide a detailed, point-by-point response to your comments and questions giving indication of the corrections performed in the text or specific motivations for not making them in the few cases where we judged differently.

REVIEWER 1

Hi author and editor,

I am glad to review this manuscript. This paper presents the application of a novel processing approach (W/D procedure) to surface wave streamer data. The SW field data test shows the advantage of the W/D processing method in surface wave data. This paper is well written. I recommend accepting this manuscript with a minor review.

The following is my details comments:

1. In figure 8, the vs and vp profile look similar. How can you get the Vp result? Please add the description in the main text.

Yes, the Vs and Vp results appear indeed similar since the Vp distribution is obtained from the Vs one with the application of the Poisson's ratio calculated from the W/D procedure (reported in Figure 8c). This last is assumed constant through the whole profile and therefore the resulting Vp velocity field is a transformation of the Vs one with similar properties. A comment was added in the paper in this respect when presenting the figure. Some comments on the implications of this assumption were already present in the discussion section of the paper.

The way in which the Vp information can be extracted through the W/D procedure via the apparent Poisson's ratio profile was already partially contained in the previous version of the paper. Following also the above general comment some more effort was performed in order to increase the description of the W/D procedure with respect to this point, without replicating available literature.

2. The dashed line in the inverted velocity result indicates the depict the river embankment in figure 2. So, I suggest adding the Stratigraphic log and geotechnical description of a figure in the inverted velocity profile, such as figure 8 and figure 9.

Thank you for the observation. Following your recommendation, the DPSH Blow Count profile was added in Figure 8 at the beginning of the survey line and some comments were addressed in the text to more specifically link the geophysical observations to the survey log.

3. This manuscript used the Monte Carlo Inversion (MCI) algorithm to invert the 1D dispersion curves. However, there are other inversion methods, such as

FWI or dispersion wave equation method. So, I suggest citing the following reference paper in the introduction section.

Thank you for the suggested and very interesting references. These alternative inversion strategies were referenced in the introduction section of the paper.

Jing Li, Z Feng, G Schuster. Wave-equation dispersion inversion. *Geophysical Journal International*, 2017, 208 (3), 1567-1578.

Yudi Pan, Lingli Gao, Renat Shigapov Multi-objective waveform inversion of shallow seismic wavefields *Geophysical Journal International*, 2020, 3: 1619-1631

4. There are two figure 1 in the main text. Please correct it.

The typo was corrected.

5. In figure 3b, the elected high energy maxima (white asterisks) is the picked fundamental dispersion curve. Because of the effect from high-order mode, how can you pick the accurate result in the high-frequency range (>30Hz). Please add some descriptions in the main text.

Thank you for the observation. Indeed, for some of the shots, a transition of the absolute energy maxima towards higher modes was observed in the high-frequency range (>30Hz), like in the example reported in Figure 3b as you correctly observe. Nevertheless, the fundamental mode can still be followed as local maxima thank to the adopted masking that allow to isolate the correct portion of the dispersion image to be considered for the automatic research of maxima, excluding the higher modes. A paragraph was added in the text to better clarify this procedure.

6. The horizontal label in figure 6, depth(m/s), maybe there is some mistake.

The typo was corrected.

7. There are two red lines in figure 7. I do not think the right side is the fitting result. Please check it.

Yes, the two red lines are correct since they both refer to the best fitting model determined from MCI. This model is represented both in terms of layered Vs and of Vs,z (the righthand side line you were referring). A clarification was added in the figure caption. Moreover, the figure has been better commented in the text with specific references to the colors used and to the meaning of the different profiles shown.

REVIEWER 2

Generally, the authors of this manuscript applied the surface wave inversion (called W/D relationship approach) to achieve a near-surface P- and S- wave velocity model that can be used to investigate the security and geomechanical strength of river embankments.

This manuscript is more likely a case study paper. Overall, the writing is well-prepared and clear. The objective of this study is pretty interesting and reasonable. In addition, the application of their surface wave inversion W/D approach on investigating the river embankments is valuable and economically sound.

Besides lacking a detailed description on W/D approach and the validation of final inverted Vp/Vs models, the manuscript is complete. This manuscript is also well organized. All figures are well prepared.

I have two main suggestions and several minor comments in follow.

Main suggestions/comments:

1. This manuscript is about an application of surface wave inversion using W/D relationship on a field dataset. One keypoint/highlight is the W/D relationship. However, there is no detailed description of W/D approach even they cited their previous works published in Geophysics. It shall be more convenient for readers to understand the W/D approach via reading its description in this manuscript rather than referring to their previous works.

Following the above general comment some more efforts were performed in order to increase the description of the W/D procedure, without replicating available literature. We think that the main computation steps are now better explained and clearer. Hope that the reviewer will be satisfied with that.

2. They finally achieved 2D inverted Vs/Vp velocity profiles for this sturdy region. However, there is no validation of such results. I strongly suggest authors perform numerical elastic waveform modeling to compare the modeled surface waves using their inverted Vs/Vp models and their observed waveforms. The numerical validation could make their work more solid and complete.

We do not agree with the reviewer that the presented velocity sections from the W/D procedure lack in validation. Comparison is specifically made in the paper, with detailed normalized differences images, to commonly adopted methods, considered as benchmarks, for Vs and Vp sections computed from seismic data. This was also specifically mentioned in the text and commented explaining eventual differences with the benchmarks. Further comments were added in the paper to specifically recall this validation approach.

By applying the proposed procedure to streamer data, the final aim of the paper is indeed to obtain in a fast and economically convenient way velocity sections equivalent to standard approaches. With this respect the waveform and dispersion computation suggested by the reviewer, even if interesting, is partially out of scope of the paper being strongly time demanding for the proposed application and not directly interesting for the embankment characterization. This comparison was moreover already performed, showing very reliable results, in Khosro Anjom et al. (2019) and Teodor et al. (2020) referenced in the text.

Some mirror suggestions

1. Abstract section

It is better to mention the application of W/D approach in the surface wave inversion. This is one highlight/keypoint of this case study manuscript.

The W/D procedure is now explicitly mentioned in the abstract of the paper.

2. Line 82, "W/D" The abbreviation "W/D" is not defined before its first appearance even I can find its definition at line 86.

Thank you for the observation. The meaning of the abbreviation is now explained since its first appearance in the text.

3. Line 81, "is proposed in this paper" Because the W/D procedure is not original developed (proposed) in this manuscript. "is propose" is not accurate and suitable here. Suggest change to "is adopted in this paper".

The statement was corrected as suggested.

4. Line 148, figure 3b, dispersion map To form the dispersion map, you may try multiple-channel nonlinear signal comparison ((Zheng and Hu 2017, Hu et al. 2019) to achieve a higher resolution dispersion map.

Thank you for the suggested and very interesting references on dispersion image approaches. These alternative approaches were referenced in the paper when discussing about dispersion image extraction.

Moreover, the measurement of dispersion curve via picking the maxima at different frequencies is better to include the measurement errors or error bars.

As explained in the text, only a single seismic shot was recorded for each position of the streamer along the embankment. Given this acquisition approach we do not have unfortunately enough information to allow for a computation of measurement error bars. No comments were added in the text in this respect. We are available to add them if the reviewer requires them mandatory.

Hu, H., M. Senkaya, and Y. Zheng. 2019, A novel measurement of the surface wave dispersion with high and adjustable resolution: Multi-channel nonlinear signal comparison. *Journal of Applied Geophysics*, 160,236-241.

Zheng, Y., and H. Hu. 2017, Nonlinear Signal Comparison and High-Resolution Measurement of Surface-Wave Dispersion. *Bulletin of the Seismological Society of America*, 107, no. 3,1551-1556.

5. Figure 5, "Vr" What is "Vr"? The trial random velocity?

Vr is the Rayleigh wave phase velocity. This is now explicitly referenced in the text. Modifications were also performed to the panel a) of the figure to avoid confusion.

6. Figure 6.

I do not understand how to estimate the apparent Poisson ratio from Figure 6 and line 210 - 214. From my understanding, the W/D relationship could be directly transformed from the dispersion curve $V_{Vs}(ff)$ at different frequencies. How to connect the Poisson ratio to W/D and V_{Vs} ? I am confused about this point.

I strongly suggest adding some mathematical descriptions on conducting the W/D relationship and Figure 6, in this section or in the appendix section, rather than just cite their previous works published in *Geophysics*, 2017.

Please see the answer to your main comment 1.

1 **Effective Vs and Vp characterization from Surface Waves streamer** 2 **data along river embankments.**

3

4 Comina C.¹, Vagnon F.¹, Arato A.², Antonietti A.²5 ¹Dipartimento di Scienze della Terra, Università degli studi di Torino, Torino (IT)6 ²Techgea S.r.l., Torino (IT).

7

8

9 **ABSTRACT**

10

11 River embankments are linearly extended earth structures built for river flood protection. Their
12 continuity and uniformity are fundamental prerequisites to ensure and maintain their protection
13 efficiency. Weakness points usually develop in localized areas where geotechnical variability is
14 present in the embankment body or in the underlying subsoil. Given their significant length, and the
15 localized nature of weakness points, the characterization of river embankments cannot therefore
16 rely on local geotechnical investigations but requires the application of efficient and economically
17 affordable methods, able to investigate relevant lengths in a profitable way. This is even more
18 essential when the investigations are conducted near, or in foresee of, significant flood events, when
19 timing of the surveys is essential. In this paper the application of a procedure ([W/D procedure](#)) for
20 the seismic characterization of river embankments, specifically designed for surface waves streamer
21 data, is presented. The [W/D](#) procedure allows the combined definition of 2D shear (Vs) and
22 compressional (Vp) wave velocity models and can be developed in order to be automated as a fast
23 imaging tool. Its application to the characterization of a test site (Bormida river embankment,
24 Piedmont Region, Italy) is presented. It is also shown that the obtained results are comparable to
25 standard seismic processing approaches with the advantage of reduced survey time and increased
26 efficiency, giving preliminary results directly in the field.

27

28 **Article Highlights:**

- 29 • Effective Vs and Vp information are extracted from surface waves streamer data;
- 30 • An automated procedure for the seismic characterization of river embankments was
31 developed;
- 32 • The procedure is demonstrated comparable to standard seismic processing approaches;
- 33 • Advantages in survey time and efficiency is highlighted.

34

35 **Keywords:** surface waves, seismic characterization, river embankments.36 **Corresponding author:** Cesare Comina, cesare.comina@unito.it

37

38 **1. INTRODUCTION**

39 River embankments are linearly extended earth structures constructed to serve as flood control
40 systems during large rain events. A proper characterization of the embankment body is essential to
41 verify its uniformity and to monitor the occurrence of possible integrity losses which could
42 undermine its stability. In recent years, frequency and magnitude of extreme flood events have been
43 rapidly increasing in Central America, Southern Europe, and in Italy because of climate change.

44 Moreover, the poor maintenance of hydraulic structures, ~~which~~ mostly ~~are~~ reaching their design
45 service life, makes the adoption of specific interventions of paramount international relevance.

46 Given the significant length extension of these structures, and the localized nature of weakness
47 points, the characterization cannot rely only on local geotechnical investigations but requires the
48 application of efficient and economically affordable methods, able to investigate the whole
49 embankments in a profitable way. Moreover, geotechnical investigations usually require invasive
50 procedures (such as boreholes, penetration tests, etc) that are both expensive and time-consuming.
51 With this respect non-invasive, rapid and cost-effective methods are desirable to identify higher
52 potential hazard zones.

53 Among the available non-invasive geophysical methods (Chao et al., 2006; Bergamo et al., 2016;
54 Takahashi et al., 2014; Sentenac et al., 2018), the seismic ones have peculiar advantages for the soil
55 characterization. Seismic velocities, and particularly shear wave velocity (Vs), are directly related
56 to the dynamic stiffness of the material, which is an important mechanical parameter for the
57 recognition of soil layers. Moreover, in the field of geotechnical engineering, huge research effort
58 has been spent on the correlation of Vs to parameters obtained from standard geotechnical tests. Site
59 specific and general correlations exist to porosity, plasticity index, to the shear modulus at higher
60 strains and to standard geotechnical in situ tests such as cone penetration, standard penetration and
61 dilatometer tests (e.g. Kramer, 1996; Samui, 2010; Foti et al., 20014).

62 Among the seismic methods the multichannel analysis of surface waves (MASW), based on the
63 Rayleigh wave dispersion curve (DC) analysis, is considered the most effective for the
64 determination of Vs profiles. This method can be efficiently applied to seismic streamer data
65 dragged along embankments and overall linear earth structures. This allows the determination of
66 several Vs profiles to offer an almost 2D representation of the velocity field. Several literature
67 applications of this methodology are available along embankments, river dykes and earth dams (e.g.
68 Lutz et al., 2011; Lane et al., 2008; Min and Kim, 2006). Eventually, MASW surveys can be used
69 in combination with geoelectrical and geotechnical methods to allow for more complete
70 characterization (e.g. Samyn et al., 2014; Busato et al., 2016; Bièvre et al., 2017; Rahimi et al.,
71 2018; Arato et al. 2020).

72 The main limitations of this methodology are related to the high non-linearity of the DC inversion
73 procedure and to the lack of compressional wave velocity (V_p) information. Several global
74 inversion approaches have been proposed for the DC inversion (e.g. [Socco and Boiero, 2008](#)), with
75 the aim of tackling the problem of non-uniqueness of the solution. More elaborated inversion
76 strategies for reconstructing 2D shear wave velocity sections including waveform information (e.g.
77 wave-equation dispersion inversion (WD), Li et al., 2017, or multi-objective waveform inversion
78 (MOWI), Pan et al., 2020) have been also proposed. Nevertheless, all these approaches are highly
79 time consuming, particularly for increasing number of DCs to be analysed, and can be adopted only
80 in the post-processing stage, not allowing for an effective in situ characterization. The lack of V_p
81 information can also be a disadvantage since V_p is known to be correlated with saturation levels
82 and related ~~Poisson's~~Poisson ratio of the materials. This last could be indeed an important
83 parameter to be determined along river embankments, to complete the characterization.

84 To overcome these limitations, the application of a new procedure ([Socco et al., 2017](#); [Socco and](#)
85 [Comina, 2017](#)) for the analysis of Rayleigh wave fundamental mode DC is ~~proposed~~adopted in this
86 paper. This procedure is based on the relationship between Rayleigh wave wavelength and
87 investigation depth (W/D procedure) ~~is based on~~and exploit the higher sensitivity of the DCs to
88 time-average shear wave velocity ($V_{s,z}$) than to layered velocity profiles and ~~to~~ the sensitivity of
89 the Rayleigh wave skin depth to V_p . The W/D procedure allows the determination of both 2D V_s
90 and V_p sections from the DCs using a direct data transform approach. ~~A~~The relationship between
91 the wavelength of the Rayleigh wave fundamental mode and the investigation depth (W/D
92 relationship) is estimated through a reference V_s and $V_{s,z}$ profile and used to directly transform all
93 DCs into V_s profiles. The sensitivity of the W/D relationship to ~~Poisson's~~Poisson ratio is moreover
94 exploited to obtain also V_p profiles along the studied embankment. The procedure has already
95 demonstrated its reliability both on synthetic and real data, producing V_s and V_p models which
96 allow a reliable waveform matching in comparison to benchmarks ([Khosro Anjom et al., 2019](#)) and
97 effective full waveform inversion starting models (~~Khosro Anjom et al., 2019~~; [Teodor et al., 2020](#)).

98 Another significant advantage of the proposed W/D procedure is that, being a data transform
99 approach, it does not have particular computational requirements. In principle, it could therefore be
100 applied also during in situ measurement campaigns for a fast imaging of the seismic properties of
101 the studied embankment. This ~~result~~products ~~in~~ a strong reduction of survey time and increased
102 efficiency. In this paper, the procedure is specifically implemented for surface waves streamer data
103 and its application to the characterization of a test site (Bormida river embankment, Piedmont
104 Region, Italy) is presented. It is shown that the obtained results are comparable to standard seismic

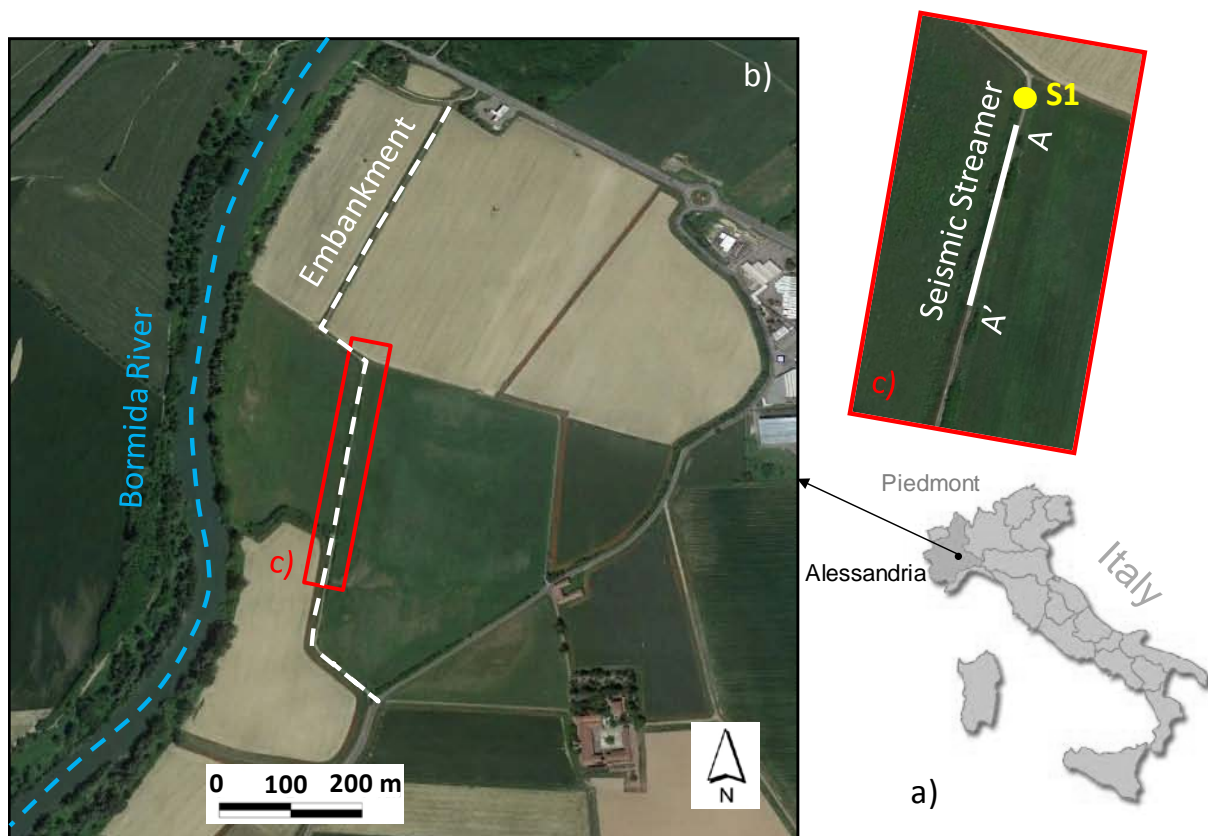
105 processing approaches with the advantage of reduced survey time and increased efficiency, and that
106 preliminary results can be obtained directly during in situ measurements.

107

108 2. TEST SITE AND EXECUTED SURVEYS

109 The test site investigated in this paper is the right embankment of the Bormida river, east of the city
110 of Alessandria, in Spinetta Marengo municipality, Piedmont Region, NW Italy (Figure 1). The
111 embankment is separated from the river by the presence of a 200 m wide floodplain that serves as
112 expansion area during floods (Figure 1). The top of the embankment rises about 9 m from the free
113 surface of the river, and about 3 m from the floodplain. The soil composition of the embankment
114 (embankment body and foundation) was obtained by available geotechnical tests: a borehole,
115 executed on the top of the embankment in correspondence of an embankment curve (S1, in Figure 1
116 inlet) and a dynamic penetration super heavy test (DPSH) executed in the proximity of the borehole.
117 Both the borehole and DPSH interested ~~both~~ embankment body and foundation soil till about 16 m
118 depth.

119

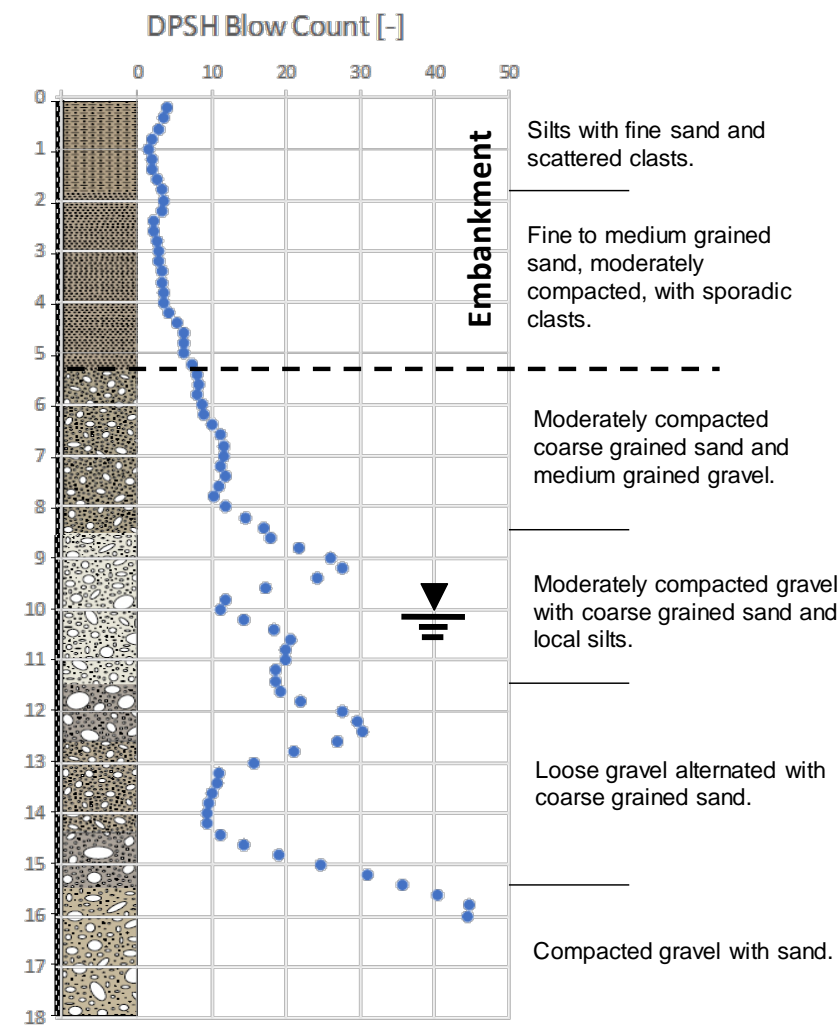


120 **Figure 1 – Location of the test site: a) north western Italian Po plain, Piedmont region, near the city of**
121 **Alessandria, b) detail of the studied embankment and c) executed surveys.**

122 The geotechnical setting (Figure 2) can be synthesized as constituted by silts with fine sands and
123 scattered clasts changing to fine to medium grained sands, moderately compacted, with sporadic

124 clasts, up to about 5.3 m depth (embankment body) overlaying a coarse sand and gravel formation
125 moderately to medium compacted with intercalated silts and local compaction reduction with depth.
126 At the moment of execution of the borehole (November 2007) the water table was reported at about
127 10 m depth from the embankment top; given the height of the river, the water table is therefore
128 supposed to be fed by the river and its elevation strictly dependent on the water level within the
129 river.

130 As it can be observed in the stratigraphic log, the transition from embankment body to natural
131 subsoil does not appear to be particularly sharp. This can be an indication that the construction
132 procedure did not involved relevant reworking of the first subsoil and that lateral differences in
133 depth and nature of this contact could be present along the embankment. Taking as reference the
134 DPSH result, local eventual differences along the embankment body will be investigated using
135 seismic streamer data dragged along a specific portion of the embankment (Figure 1).



136

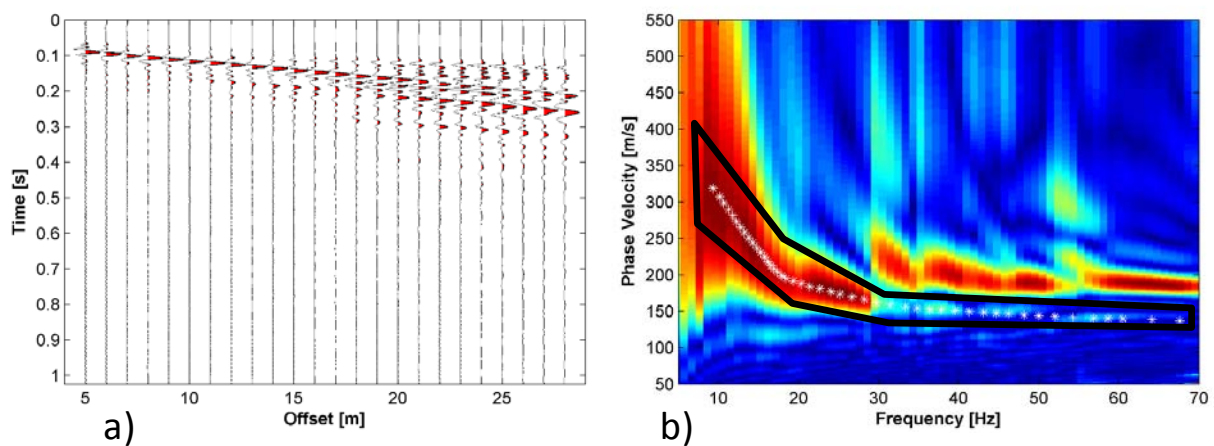
137 **Figure 1-2** – Stratigraphic log and geotechnical description of the encountered formations with
138 evidence of the DPSH results.

139 An embankment sector of about 90 m, south with respect to the S1 borehole (Figure 1), was
140 investigated in May 2019 with a seismic land streamer constituted of 24, 4.5 Hz vertical geophones
141 mounted on coupling sliders at 1 m spacing. The streamer was dragged by a pick-up truck and was
142 moved along the studied reach at 2 m steps; for each moving step a single seismic shot was
143 registered. The seismic source was a 40 kg accelerated mass mounted on the pick-up back; a 5 m
144 source offset was adopted in the acquisitions. The streamer was connected to a DaQLink IV
145 (Seismic Source, 2016) acquisition device on the pick-up truck, storing the data in a survey laptop
146 and eventually applying pre-processing steps. Seismograms were acquired with a 0.5 ms sampling
147 interval, -50 ms pretrig and 1.024 s total recording length. A total of 45 seismograms were therefore
148 acquired during the survey. On these data several processing steps were applied for the definition of
149 2D Vs and Vp models with the proposed W/D procedure.

150

151 3. METHODOLOGY

152 An example seismic shot is reported in Figure 3a. The used source and streamer setup allowed the
153 acquisition of high-quality data, with clear evidence of surface waves dispersive pattern and also
154 particularly evident first arrivals of compressional waves.



155

156 **Figure 3 – Data processing procedures on acquired seismograms: a) example seismic shot, b)**
157 **dispersion curve extraction with evidence of the applied mask (black line) and selected high energy**
158 **maxima (white asterisks).**

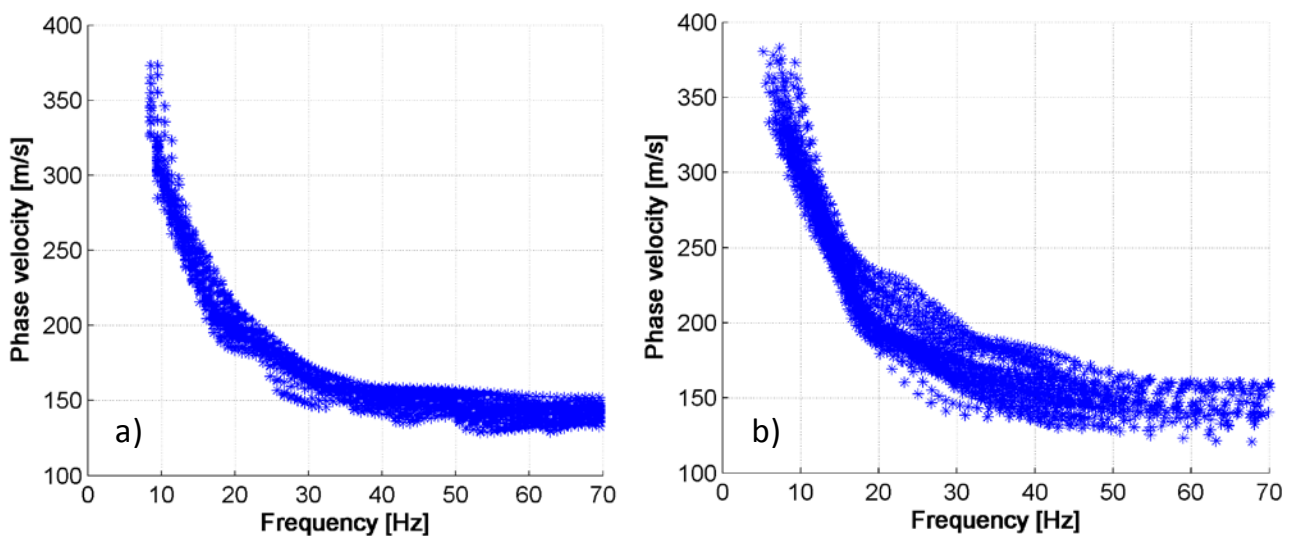
159 DCs extraction was performed with two different procedures: first, the dispersion image for each
160 seismogram was obtained by means of a phase-shift approach (Park et al., 1998) implemented in
161 MATLAB® routines. The phase-shift approach has demonstrated to maintain very good
162 performances even when a limited number of traces is considered (Dal Moro et al., 2005).

163 Alternatively, to further improve the accuracy of dispersion measurement, a multi-channel

164 nonlinear signal comparison (MNLSC, Hu et al., 2019) can be adopted, producing high and
165 adjustable resolution among a wide detected frequency range.

166 On the dispersion image this image the zone pertinent to the fundamental mode propagation was
167 selected with a mask (black line in Figure 3b) and energy maxima were automatically searched
168 within this area (white asterisks in Figure 3b). The mask selected for the first shot can be either
169 automatically used for all the following shots (automatic procedure) or partially adjusted to follow
170 eventual variations in the energy distribution (semi-automatic procedure). In the first case a rough,
171 but fully automated, DCs selection is obtained, in the second case a more refined, but more time
172 consuming, analysis is allowed, to better evidence eventual lateral variations. On both these selected
173 DC groups eventual smoothing and manual outlier removal can be applied to obtain more
174 continuous and reliable curves.

175 In Figure 4 the resulting DCs selected for all the shots from automatic and semi-automatic
176 procedures are reported. For some of the shots a transition of the absolute energy maxima towards
177 higher modes was observed in the high-frequency range (e.g. frequencies higher than 30Hz in
178 Figure 3b). Nevertheless the fundamental mode can still be followed as local maxima thank to the
179 adopted mask that allowed to isolate the correct portion of the dispersion image to be considered,
180 excluding the higher modes from the maxima searching. It can be evidenced that the DC ranges are
181 very similar with corresponding velocity transition. Nevertheless, the semi-automatic procedure
182 (Figure 4b) shows higher variability for the medium-high frequency range (shallower layers) as a
183 result of the application of a variable mask. Most of the results reported in the paper refer to the
184 DCs selected with this approach. In the discussion section some comparisons are however presented
185 with the results obtainable with the automatic procedure also.



186

187 **Figure 4 – DCs selected for all the shots: a) automatic procedure and b) semi-automatic procedure.**

188 The application of the W/D procedure to the extracted DCs requires the knowledge of a single V_s
189 and $V_{s,z}$ reference profile along the seismic line together with its associated DC. This profile can be
190 either extracted from the data themselves, by performing the inversion of a representative DC
191 among the ones extracted, or it can be obtained by independent seismic or geotechnical data.

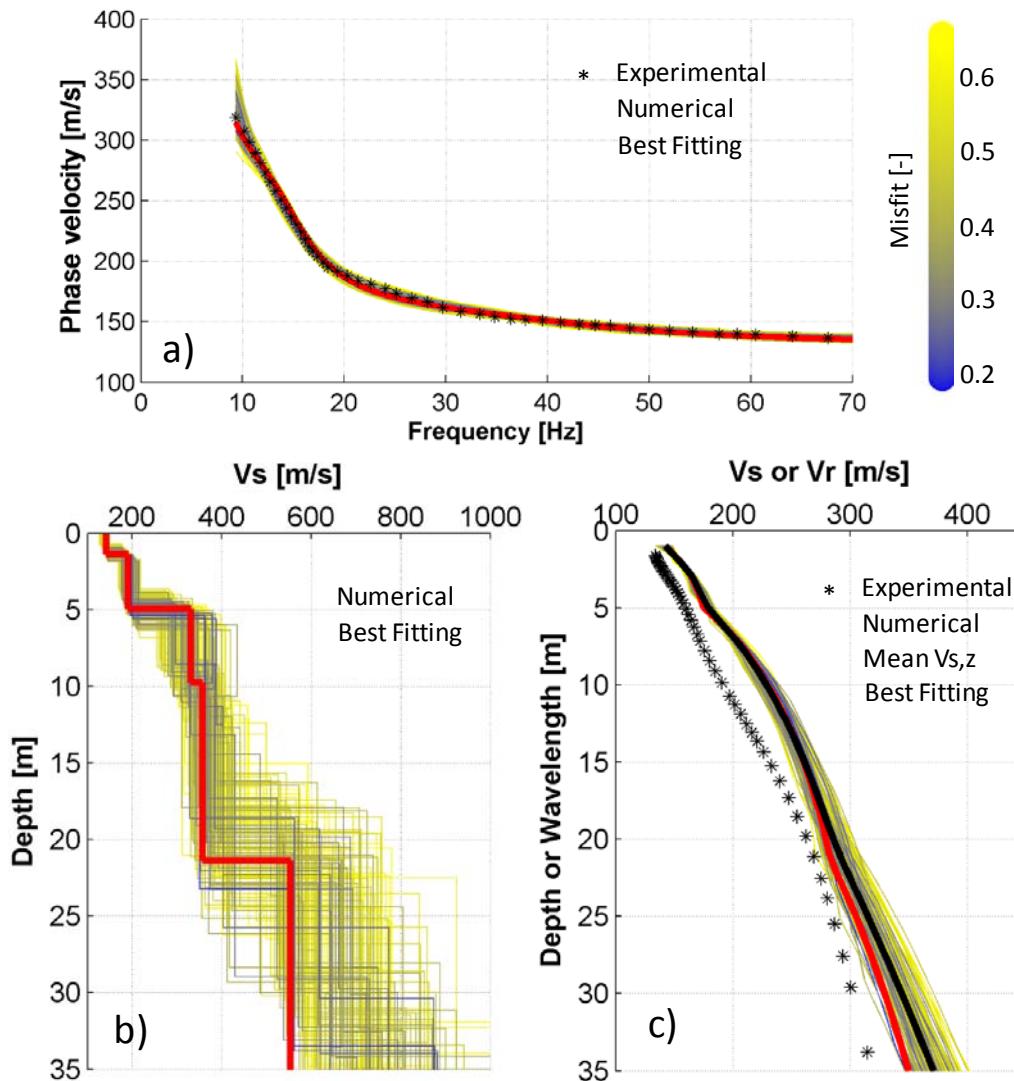
192 In this paper the first method was adopted using a Monte Carlo Inversion (MCI) algorithm (Socco
193 and Boiero, 2008) which efficiently limits potential non-uniqueness of the solution and results in
194 reliable V_s and $V_{s,z}$ profiles. The inversion implies the definition of a wide model space by
195 selecting ranges for each model parameter (V_s , thicknesses and the Poisson ratio ~~offer~~ for each layer)
196 and performing random sampling (10^5 profiles) among these ranges. Please note that, in order to
197 allow for the W/D procedure to be applied, also Poisson ratio of each layer is considered as a model
198 parameter, contrary to what usually performed in the inversion of DC curves.

199 Example application of the inversion process to the DC reported in Figure 3b, which was selected
200 as reference, is reported in Figure 5. It can be observed that the set of statistical equivalent profiles
201 selected from the MCI assess the presence of a contrast at the bottom of the embankment around 5
202 m depth (Figure 5b). This set of profiles, and their correspondent numerical DCs, is represented in
203 Figure 5 with a relative misfit representation based on the absolute difference between each profile
204 misfit and the best fitting one (in red in Figure 5).

205 It can also be noted that the higher variability in terms of V_s profiles (Figure 5b) strongly reduces
206 when the time average shear wave velocity is considered ($V_{s,z}$, in Figure 5c). With this respect the
207 best selected profile (in red in Figure 5c) and the mean of the statistical set (in black in Figure 5c)
208 almost superimpose for the top portion of the profile. Socco and Comina (2015) have already shown
209 that the non-uniqueness of the DC inversion very slightly affects the estimation of time-average
210 velocity, and hence, the $V_{s,z}$ obtained from inverted profiles is very robust. Nevertheless, given the
211 increased uncertainty at the bottom of the profile, the following analyses were limited to 20 m
212 depth, which is enough ~~for the studied test site~~ for investigating both the embankment and a
213 significant portion of the foundation subsoil at the studied test site.

214 Using the reference V_s and $V_{s,z}$ profiles and all the extracted DCs, the proposed data transform
215 procedure is then applied as following: i) the estimated $V_{s,z}$ and its corresponding DC are used to
216 compute the reference W/D relationship; ii) the reference W/D relationship is used to transform all
217 DCs into $V_{s,z}$ models; iii) an apparent Poisson ratio is estimated using the reference W/D
218 relationship and the reference V_s model; iv) using the apparent Poisson ratio, each $V_{s,z}$ profile is
219 transformed into a $V_{p,z}$ profile; v) all the reconstructed $V_{s,z}$ and $V_{p,z}$ profiles are ~~then~~-transformed
220 into V_s and V_p profiles with an interval velocity analysis.

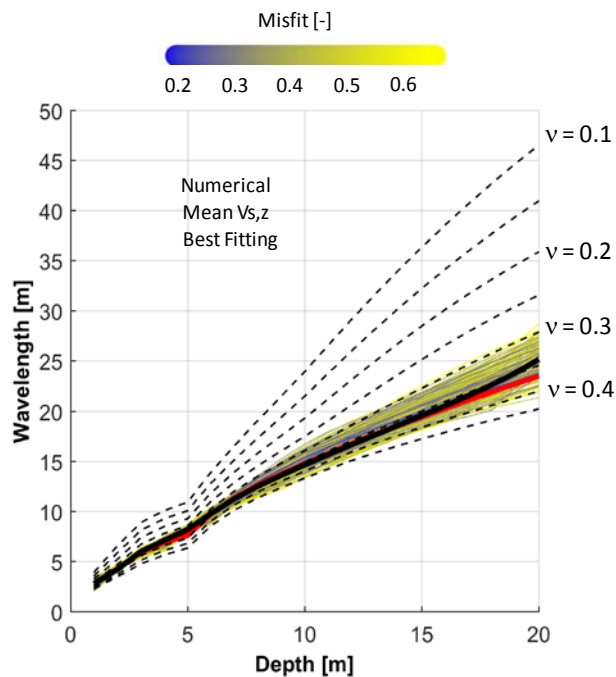
221



222

223 **Figure 5 – MCI of the reference DC curve: a) experimental and numerical dispersion curves b) best**
 224 **fitting profile and set of statistically equivalent profiles and c) experimental dispersion curve as a**
 225 **function of wavelength, time average velocities of best fitting profile and statistically equivalent**
 226 **profiles with their mean.**

227 Steps i) and iii) of the procedure require more explanations. The meaning of the W/D relationship is
 228 represented in Figure 5c: for each $V_{s,z}$ value, the wavelength (W) at which the phase velocity (V_r)
 229 of the DC is equal to the $V_{s,z}$ (see the arrows in Figure 5c) is searched for each depth (D). With all
 230 the W/D pairs at which $V_{s,z}$ and phase velocity are equal a relationship is obtained (W/D
 231 relationship. This relationship is represented in Figure 6) for the best fitting profile (in red), for the
 232 mean of the statistically equivalent profiles (in black) and for all the statistically equivalent profiles.
 233 Consistency of the extracted W/D relationships is evidenced.



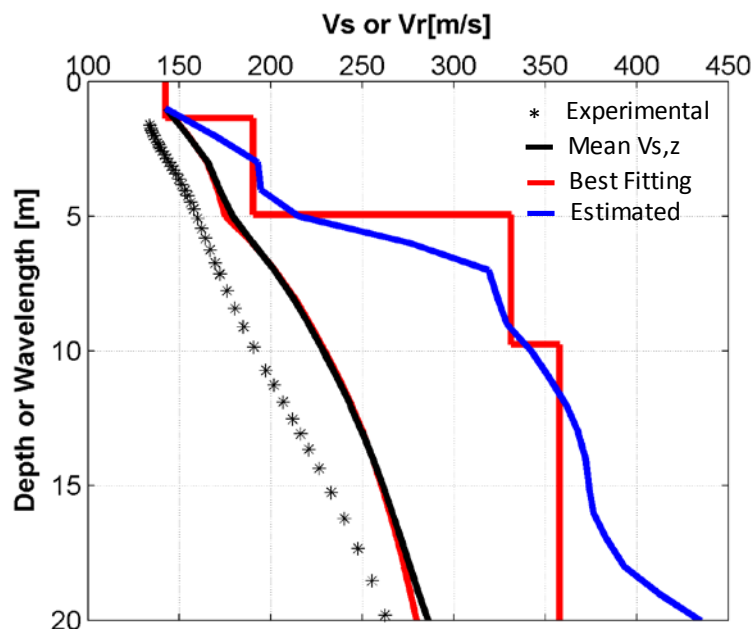
234

235 **Figure 6 – The W/D relationship for the reference DC for the best fitting profile (in red), for the mean**
 236 **of the statistically equivalent profiles (in black) and for all the statistically equivalent profiles**
 237 **compared with the ones obtained with different Poisson's Poisson ratio values. ~~Some~~ Reference**
 238 **Poisson's Poisson ratio values are indicated on the right of the plot.**

239 This relationship represents the surface waves' skin depth for increasing wavelengths and has been
 240 demonstrated (Socco and Comina, 2017) to be influenced by the Poisson's Poisson ratio of the
 241 formation. With the reference V_s and $V_{s,z}$ profiles it is therefore possible to build different
 242 synthetic W/D relationships by changing the value of the Poisson's Poisson ratio (ν) of the layers
 243 (assumed constant for all the layers). These synthetic W/D relationships are reported in Figure 6
 244 (dashed black lines) for some example values of the Poisson ratio, dashed black lines in Figure 6).
 245 It can be noted that Poisson ratio acts on the slope of W/D relationship. In particular, the slope
 246 decreases when Poisson ratio increases. Therefore the slope of the experimentally determined W/D
 247 relationship contains information on the actual Poisson ratio of the formation. -The actual apparent
 248 Poisson's Poisson ratio profile of the formation can be therefore searched by associating to each
 249 depth the value of Poisson's Poisson ratio that corresponds to the linear interpolation between the
 250 upper and lower nearest synthetic constant Poisson's ratio W/D relationships. In this way an
 251 apparent Poisson ratio profile with depth can be obtained for the reference DC. This profile can be
 252 later used to transform all the $V_{s,z}$ profiles into $V_{p,z}$ profiles allowing for a 2D V_p section to be
 253 later computed.

254 An example application of the W/D procedure to the reference DC is reported in Figure 7. It can be
 255 observed that the $V_{s,z}$ of the best fitting profile (continuous red line in Figure 7) and the mean $V_{s,z}$

256 of the statistical set (continuous black line in Figure 7) almost superimpose for the first 20 m depth.
 257 It can be ~~observed~~ also noted that the W/D procedure allows the estimate of a Vs model (in blue in
 258 Figure 7) very near to the best fitting one (layered red line in Figure 7) obtained from the MCI of
 259 the DC. The model obtained with this procedure has also the advantage of not making any
 260 assumption with respect to the number of layers of the profile. For this reason, it can result
 261 smoother with respect to the layered profile but also more correspondent to the actual geotechnical
 262 situation below the embankment. Particularly, it can be observed that the transition from
 263 embankment body to bottom layers with this estimated profile appear to be more correspondent to
 264 what evidenced in the DPSH profile results (Figure 2) with respect to the sharp interface evidenced
 265 by the MCI result.



266
 267 **Figure 7 – Application of the W/D procedure to the reference DC for Vs profile determination and**
 268 **comparison with the best fitting result (both in term of layered velocity model and Vs,z) from MCI.**

269 All the Vs and Vp profiles estimated with the W/D procedure are then interpolated along the studied
 270 embankment to allow for a 2D visualization of the Vs and Vp velocities distributions. The data
 271 gridding was performed in Surfer (Golden software) with an interpolation grid of 2 m in the
 272 horizontal direction (equal to the acquisition step) and of 0.5 m in the vertical direction.

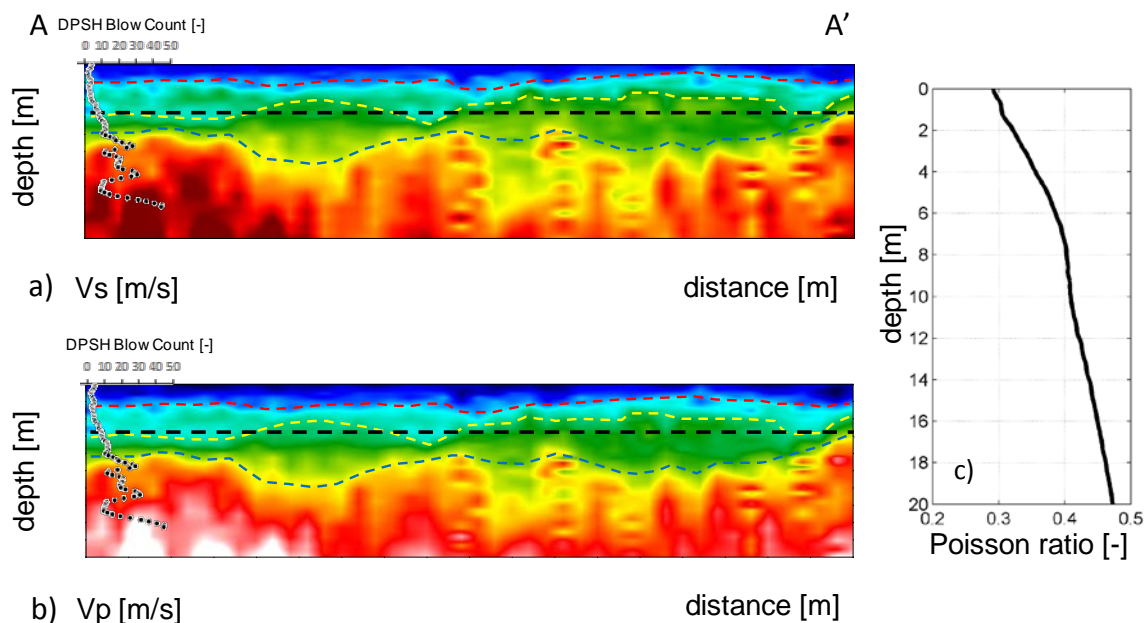
273 To validate the velocity models obtained with the application of the W/D procedure ~~the~~ the obtained
 274 results are ~~then~~ benchmarked against standard seismic processing approaches. For Vs, all the
 275 dispersion curves extracted were inverted with a laterally constrained inversion (LCI) approach
 276 (Auken and Christiansen, 2004; Socco et al., 2009). For this inversion, the same number of layers of
 277 the MCI was assumed. For Vp, processing was carried out by picking the first breaks on each

278 acquired seismogram, picked first breaks were then interpreted in tomographic approach with the
279 use of the software Rayfract ([Intelligent Resources Softwares Inc.](#)).

280

281 4. RESULTS

282 Results of the application of the W/D procedure are reported in [Figure 8](#). Particularly, the V_p result
283 is obtained from the V_s one with the application of the apparent Poisson ratio obtained from the
284 W/D procedure. This last is assumed constant through the whole profile and therefore the resulting
285 V_p velocity field is a transformation of the V_s one with similar properties. Both V_s and V_p sections
286 can discriminate the transition from the shallow silts and sands to the bottom gravels along the
287 embankment and to delineate the embankment bottom. Coherently with the borehole results and
288 geotechnical tests ([Figure 2](#)) this transition falls, on the left side of the sections, where the surveys
289 are nearer to the geotechnical tests (the DPSH Blow Count profile is also reported in [Figure 8a](#) and
290 [b](#)), around 5.3 m depth.



291

292 **Figure 8 – Results of the application of the W/D procedure to extracted DCs (section A-A’): a) V_s**
293 **section, b) V_p section and c) resulting Poisson’s Poisson ratio. On both the sections the supposed depth**
294 **of the embankment is also reported (dashed black line) together with coloured dashed lines, derived by**
295 **the velocity models, indicating the transition between the shallow silts and sands (in red), the thickness**
296 **of the embankment (in yellow) and the transition to compacted gravels and sands (in blue). The DPSH**
297 **Blow Count profile is also reported at the beginning of the sections.**

298 However, along the embankment a variation of the depth of this interface can be evidenced.
299 Particularly, localized anomalies appear in the V_s section suggesting an increase in the depth of the

300 shallow silts and sands of the embankment (yellow dashed line in Figure 8) around 40 m
301 progressive distance. Conversely, the depth of the interface appears to be shallower in the
302 progressive distance range between about 50 to 80 m.

303 Seismic surveys are also able to depict the transition (red dashed line in Figure 8) from silts with
304 fine sands and scattered clasts to fine to medium grained sands, as reported from the borehole and
305 DPSH results, within the embankment. A deeper increase in velocity is also observed around 8 m
306 depth on the left side of Figure 8, were the transition to more compacted gravels (blue dashed line
307 in Figure 8) is evidenced by borehole ~~results~~ and DPSH results geotechnical tests (Figure 2). This
308 more compacted formation appears however to increase its depth along the section moving away
309 from the borehole and showing on average lower velocity values. Localized velocity inversions are
310 also partially observable below 8 m in the leftmost portions of the Vs section. This evidence again
311 well compares with what reported by the DPSH results (~~Figure 2~~).

312 Notwithstanding the information on the position of the water table at the site (around 10 m) the
313 range of Vp velocities extracted by the procedure ~~depths~~ does not report, for increasing depths,
314 velocity ranges usually attributed to saturated materials (i.e. around 1400-1500 m/s). It must be
315 underlined that the time span between the two surveys is relevant (from November 2007 to May
316 2019) so that eventual variations on the water table depth could be present. Nevertheless, the
317 Poisson's Poisson ratio profile extracted with the W/D procedure (Figure 8c) shows a marked
318 increase nearly around 10 m exceeding the 0.4 value and tending to 0.5. Poisson ratio of saturated
319 soils is usually reported to be ~~indeed~~ in this ~~last~~ range (Boore, 2007). It must be underlined that the
320 Poisson Poisson ratio profile here presented is the interval Poisson ratio obtained through the Vp/Vs
321 ratio of the resulting models. This is different from the apparent Poisson ratio that is estimated in
322 the W/D procedure (Figure 6) for the DC transformation.

323 Results of the LCI processing of the extracted dispersion curves are reported in Figure 9a. A good
324 convergence of the inversion was obtained with LCI resulting in a final RMS error of 1.7%.

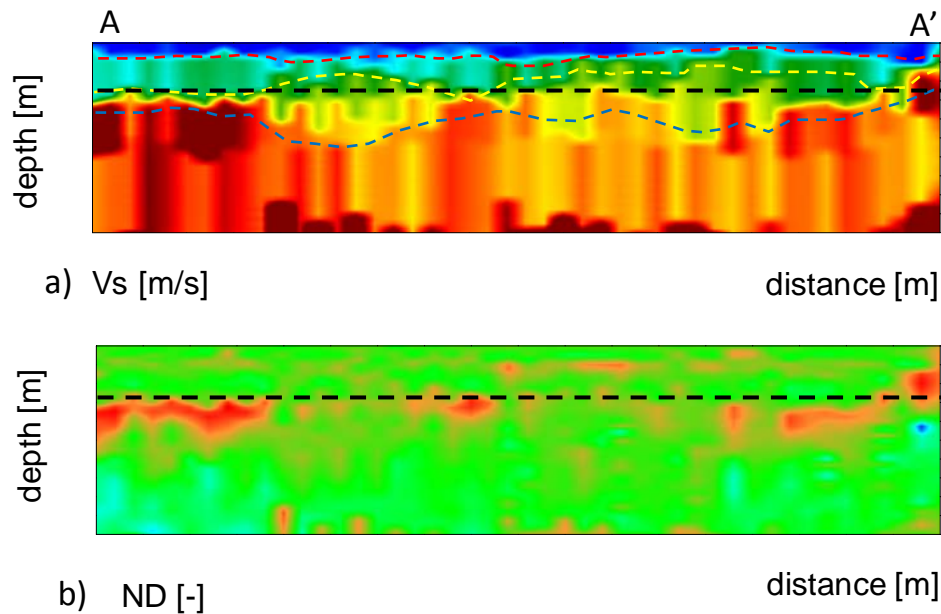
325 The comparison of the LCI result with the W/D procedure is performed in Figure 9b in term of
326 normalized differences, taking as reference the LCI results, with the formula:

$$327 \quad ND = \frac{V_{i,LCI} - V_{i,WD}}{V_{i,LCI}} \quad (1)$$

328

329 were $V_{i,WD}$ is the velocity value obtained from the W/D procedure and $V_{i,LCI}$ is the velocity value
330 obtained from the LCI in each location within the models. Therefore, positive values of the
331 normalized difference indicate zones where the W/D procedure underestimate the velocity, negative
332 values indicate the opposite. To allow computing the normalized differences in each point of the

333 models also layered LCI results were gridded with the same interpolation scheme of the W/D
334 procedure results.

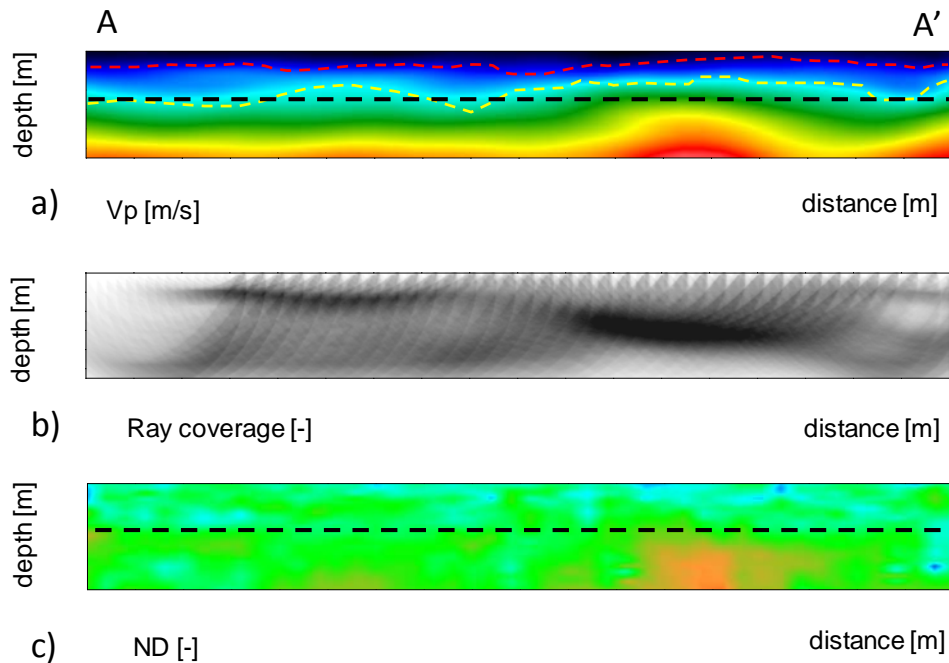


335

336 **Figure 9 – Results of the LCI of the extracted DCs (section A-A’): a) Vs section and b) Normalized**
337 **differences with the Vs results of the W/D procedure. On both the sections the supposed depth of the**
338 **embankment is also reported (dashed black line). Over the LCI section, the interfaces evidenced by the**
339 **W/D procedure indicating the transition between the shallow silts and sands (in red), the thickness of**
340 **the embankment (in yellow) and the transition to compacted gravels and sands (in blue), are**
341 **superimposed.**

342 **Figure 9** shows that the Vs velocity range obtained using LCI inversion is comparable with that
343 from the W/D procedure. The interfaces evidenced by the W/D procedure are reported for
344 comparison over the resulting Vs image. Similar variability in the depth of the interfaces is noted.
345 As an example, both the increased depth of shallower silts and sands around progressive 40 m and
346 the shallower depth of the embankment in the progressive distance range between about 50 to 80 m
347 are confirmed. Most of the normalized differences among the W/D and LCI models fall within a
348 $\pm 10\%$ range indicating the good correspondence of the two results. The only portions of the section
349 affected by higher positive normalized differences cannot be attributed to errors in the W/D
350 procedure, but to the layering assumption in the LCI. The layered discretization adopted in the LCI
351 can indeed result in an overestimation of the velocity near the layer boundaries (see also **Figure 7**
352 for comparison). Most of the higher difference values fall indeed near the embankment/foundation
353 soil interface where the layered profile results from LCI tend to give a sharper transition than the
354 W/D result.

355 Results of the tomographic inversion of picked first arrivals are reported in [Figure 10](#) and
 356 compared, in term of normalized differences, with the V_p results obtained with the W/D procedure.
 357 The same equation 1 was adopted for the computation of normalized differences with V_p values
 358 from W/D procedure and first arrivals tomography (these last substituting the LCI values in
 359 equation 1).



360

361 **Figure 10 – Results of the first break tomography (section A-A’): a) V_p section, b) Ray coverage along**
 362 **the section and c) Normalized differences with the V_p results of the W/D procedure. On both the**
 363 **sections the supposed depth of the embankment is also reported (dashed black line). Over the**
 364 **tomography the first two interfaces evidenced by the W/D procedure, indicating the transition**
 365 **between the shallow silts and sands (in red), the thickness of the embankment (in yellow), are**
 366 **superimposed.**

367 From [Figure 10](#) it can be observed that, given the reduced length of the streamer adopted, the depth
 368 of investigation of the tomography is limited to about 10 m, or even less in some portions.
 369 Nevertheless, within this depth, a high ray coverage is obtained in most of the section by the
 370 combined elaboration of all the shots. A good convergence of the inversion was obtained with a
 371 resulting RMS error of 2.7% after the final iteration.

372 Again, from [Figure 10](#) it can be observed that the tomographic inversion depicts the same velocity
 373 range compared to the one obtained with the W/D procedure. Given the reduced investigation depth
 374 of the tomography only the first two interfaces evidenced by the W/D procedure are reported for
 375 comparison over the resulting V_p image. Similar variability in the depth of these two interfaces is
 376 noted. As an example, both the increased depth of shallower silts and sands around progressive 40

377 m and the shallower depth of the embankment in the progressive distance range between about 50
378 to 80 m are confirmed. Being based on relatively long-path raytracing, the tomographic result
379 shows generally a reduced lateral resolution in the identification of the velocity variations within the
380 section.

381 Most of the normalized differences, also for V_p , fall within a $\pm 10\%$ range indicating the good
382 correspondence of the two results. The only portion of the section showing higher normalized
383 differences can be attributed to a lower ray coverage zone (see [Figure 10b](#) below 7 m at about 55 to
384 70 progressive distances) making the assumed V_p values less reliable in the tomography. Given its
385 shallower investigation depth, also the tomography does not highlight a marked increase of V_p
386 values, at the bottom of the model, attributable to the presence of the water table.

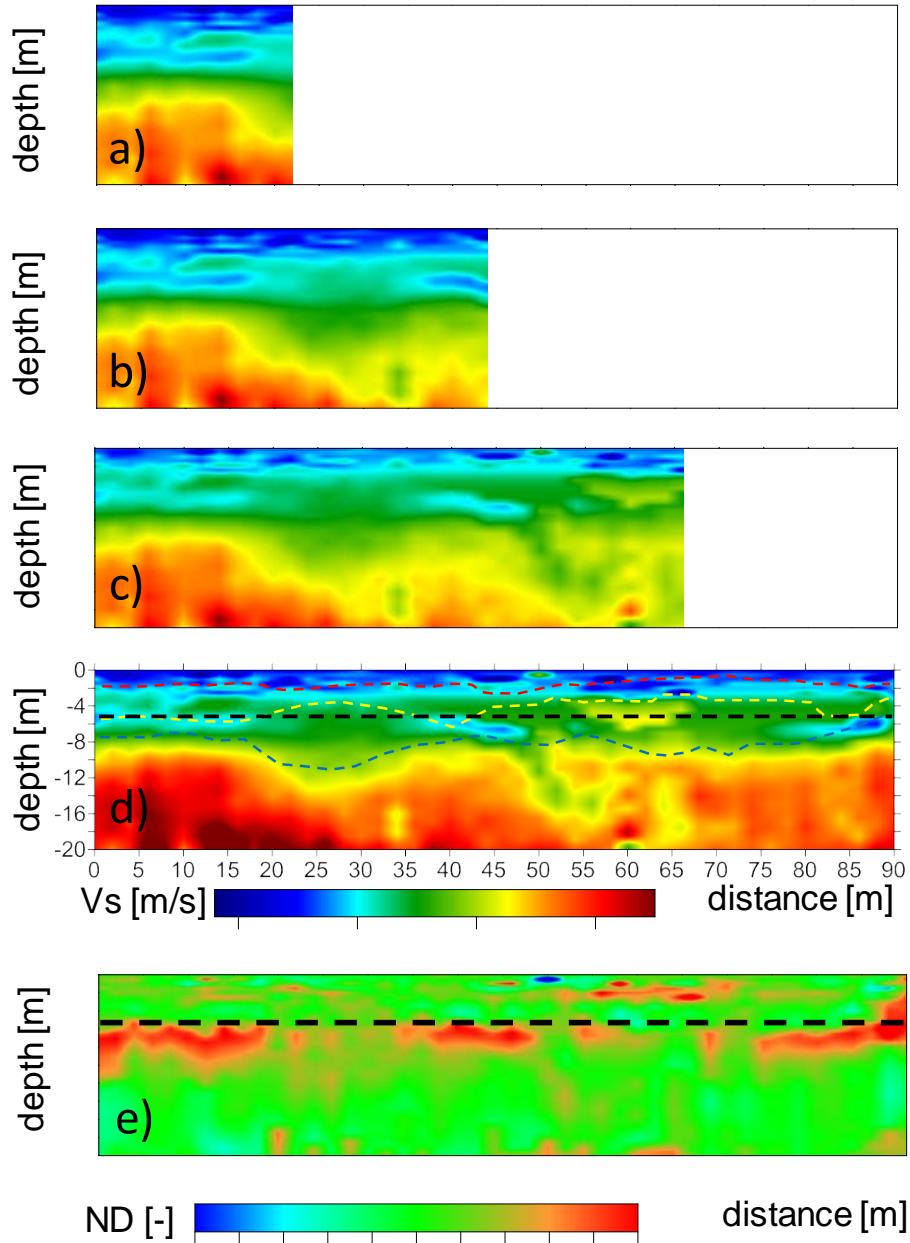
387

388 5. DISCUSSION

389 It was shown in the paper that the results obtainable with the W/D procedure are comparable both in
390 terms of V_s and V_p to standard seismic processing approaches. This comparison validates therefore
391 the application of the W/D procedure. It was observed, in the presented case study, that most of the
392 normalized differences between the W/D procedure and both LCI and first arrivals tomography fall
393 within a $\pm 10\%$ range, indicating the good correspondence of the two results. Higher normalized
394 differences along the sections can be attributed to different resolution or underlying
395 methodological assumptions among the methods and cannot be considered as an error in the W/D
396 procedure. Therefore, the W/D procedure can be established as a reliable alternative to the methods
397 here compared for the characterization of embankments and overall linear earth structures.

398 The W/D procedure has also main advantages with respect to usually seismic processing
399 approaches applied to the data obtained from similar surveys: i) being a data transform approach it
400 does not requires relevant processing and time consuming interpretations; ii) it does not make any
401 assumption with respect to the number of layers present along the investigated embankment and iii)
402 allow the combined estimation of V_s and V_p for increased depths given the same acquisition setup.
403 Particularly the first advantage is important if the speed of the surveys is considered, for example in
404 situations in which a fast and preliminary evaluation of the state of health of an embankment is
405 required. This can be the case of surveys conducted after, or in foresee of, significant rain and/or
406 flood events. In these conditions the W/D procedure, applied to the fully automated extracted DCs
407 ([Figure 4a](#)), can allow for a first, almost immediate, on site evaluation of the V_s and V_p velocity
408 field. Both the automated DC extraction step and the conversion of DC data to V_s and V_p profiles is
409 indeed a very fast process (few tens of seconds on a notebook), that outputs direct velocity models
410 while the acquisition is in progress and the streamer is dragged along the embankment.

411 An example application of this direct visualization of the Vs section during data acquisition is
 412 reported in Figure 11. It can be particularly observed that the final Vs section determined from the
 413 fully automated extracted DCs (Figure 11d) is roughly comparable with the one determined with the
 414 semi-automatic procedure (Figure 8a) with very similar depiction of the main interfaces.



415
 416 **Figure 11 – Example application of the direct visualization of the Vs section during data acquisition:**
 417 **a), b) and c) Vs sections while dragging the streamer along the embankment; d) final Vs section and c)**
 418 **Normalized differences with the LCI. In d) and e) the supposed depth of the embankment is also**
 419 **reported (dashed black line). In d) the interfaces evidenced by the semi-automated W/D procedure,**
 420 **indicating the transition between the shallow silts and sands (in red), the thickness of the embankment**
 421 **(in yellow) and the transition to compacted gravels and sands (in blue), are superimposed.**

422

423 The presence of some artefacts can be however noted within the section and can be related to the
424 reduced precision of the automatic picking of the DCs. A general increase in the normalized
425 differences with the LCI (Figure 11d) is also observed, with the presence of localized anomalous
426 local velocity values (e.g. see the shallow portion of the embankment around progressive 50 m).
427 Nevertheless, the general imaging of the Vs structure can be considered accurate enough for a first
428 estimation of the geotechnical variability at the site and a useful tool for a preliminary identification
429 of anomalous portions of the examined embankments. Given the use of the same Poisson ratio
430 profile (Figure 8c), uniform through the section, very similar considerations can be performed for
431 what concerns the resulting Vp image.

432 This direct visualization requires the knowledge of reference Vs and Vs,z profiles over which
433 calibrate the W/D relationship and the following Poisson ratio computation. In the present paper
434 these reference profiles were obtained through MCI of a reference DC. The same approach can be
435 adopted on site at the beginning of the surveys by selecting one of the clearer DCs during the first
436 shots. Nevertheless, the MCI step can be significantly time consuming and not always applied with
437 reliability on site. Possible alternative approaches would therefore require the execution of initial
438 detailed tests and interpretations through which determine with accuracy the reference profiles and
439 only later proceed with the execution of the streamer surveys. Alternatively, the reference profiles
440 can be extracted from already available geotechnical and/or geophysical surveys along the
441 embankment. With this respect the W/D procedure already showed comparable results also with
442 respect to Down Hole surveys (Socco et al., 2017).

443 Limitations of the proposed W/D procedure can be related to: i) its application to only fundamental
444 mode DC; ii) the assumption of a laterally invariable W/D relationship and Poisson ratio along the
445 embankment. With respect to the first one, the W/D procedure has been mainly developed and
446 applied to fundamental mode DC, but some attempts have been already made to include also higher
447 propagation modes (e.g. Bamarouf et al., 2017). Including higher modes showed to give advantages
448 mainly with respect to the investigation depth, even though it is a more time-consuming process.

449 However, ~~it~~ this could be a necessary step along embankments with peculiar shape dimensions,
450 since it is well known that the shape of the embankment could influence the surface wave dispersive
451 pattern and modes superposition (e.g. Karl et al., 2011). Pageot et al. (2016) have also shown that
452 internal structure layering can emphasize geometrical effects and produce DCs very different from
453 the theoretical 1D case, for both the fundamental and higher modes. In these conditions even a
454 multi-modal inversion approach could encounter some limitations to infer accurate Vs and Vp
455 models.

456 These effects have not been particularly noted at the site. As it can be observed in [Figure 3b](#), higher
457 modes are indeed present in the higher frequency range, but the fundamental mode propagation is
458 still easily recognizable as local energy maxima. This may be related to the reduced contrast
459 between the embankment body and the underlying subsoil ([Figure 2](#)) which limits the layering
460 effect and to the relevant width of the embankment (width to height ratio of about 5.5) which limits
461 the presence of 3D effects.

462 Conversely the laterally invariant assumption could be easily overcome using appropriate clustering
463 techniques on the extracted DCs that can be analysed for grouping them into subsets with
464 homogeneous properties. The W/D procedure has then to be applied to each of the identified
465 subsets. The application of this further processing step however increases again the computation
466 times and prevent a direct in situ application of the procedure but has been shown to provide
467 increased resolution in the identification of sharp lateral variations with the W/D procedure ([Khosro
468 Anjom et al., 2019; Teodor et al., 2020](#)).

469 The clustering approach was judged to be unnecessary in the presented case study given the
470 uniformity of the extracted DCs (see [Figure 4](#)) which suggest the presence of smooth depth
471 variations along the embankment but the absence of particularly sharp variations. When sharp
472 lateral variations along the embankment are the main survey target alternative identification
473 methods based on the surface waves spectral properties (e.g. [Colombero et al., 2019](#)) could also be
474 applied to the acquired streamer data.

475 To allow for a more complete characterization of the state of health of embankments, seismic data
476 are usually combined with electric resistivity data. These last can indeed give important information
477 on the variations of soil composition and water saturation, detect development of weak zones and
478 identify local anomalies potentially related to seepage. The combined use of seismic and electrical
479 data can indeed provide an effective geotechnical characterization of these earth structures, as
480 shown by several research groups that are working on their integration (e.g. [Takahashi et al., 2014;
481 Goff et al. 2015; Lorenzo et al., 2016](#)). In this respect the W/D procedure has its natural
482 development in combination with mobile electric systems allowing also a fast and effective
483 evaluation of resistivity properties (e.g. [Kuras et al., 2007; Comina et al., 2020](#)).

484 **6. CONCLUSION**

485 This paper presents the application of a novel processing approach (W/D procedure) to surface
486 wave streamer data. This approach is based on the definition a wavelength/depth (W/D) relationship
487 for surface waves and allows the combined definition of shear (V_s) and compressional (V_p) wave
488 velocities. The results obtained within the paper with the W/D procedure are comparable to
489 standard seismic processing approaches with the advantage of reduced survey time and increased
490 efficiency. It was shown in the paper as the W/D procedure can be developed in order to be
491 completely automated and used as a fast in situ imaging tool along embankments for preliminary
492 evaluations on their state of life.

493 Processing of the seismic streamer data yielded to an effective characterization of the V_s and V_p
494 velocity field along the studied embankment. The origin and properties of the anomalies
495 encountered could be better studied with the use of local geotechnical investigations to provide a
496 more specific knowledge on the state of life of the embankment. The produced seismic sections, if
497 properly calibrated with the few independent geotechnical tests available, can be nevertheless used
498 for preliminary stability evaluations also in portion of the embankment non directly covered by
499 geotechnical tests.

500 Further studies, already planned and partially executed, include the application of the W/D
501 procedure to different embankments shapes with the eventual inclusion of higher modes in the
502 interpretation. Moreover, the combined acquisition of electrical resistivity data, even with
503 innovative acquisition approaches, will allow the contemporary execution of resistivity and seismic
504 surveys with even more reduced survey time and increased knowledge on the state of health of the
505 embankments due to the acquisition of the different complementary parameters.

506 **ACKNOWLEDGMENTS**

507 This work has been funded by FINPIEMONTE within the POR FESR 14/20 "Poli di Innovazione - Agenda
508 Strategica di Ricerca 2016 - Linea B" call for the project Mon.A.L.I.S.A. (313-67). Authors thank Daniele
509 Negri for helping during acquisition surveys.

510 **REFERENCES**

- 511 1. Arato A., Naldi M., Vai L., Chiappone A., Vagnon F. and Comina C. (2020) Towards a Seismo-Electric
512 land streamer, submitted for the 6th International Conference on Geotechnical and Geophysical Site
513 Characterization, 7-11 September 2020, Budapest.
- 514 2. Auken, E., and A. V. Christiansen, 2004, Layered and laterally constrained 2D inversion of resistivity
515 data: *Geophysics*, 69, 752–761.
- 516 3. Bamarouf, T., Socco, L.V. & Comina, C., 2017. Direct Statics estimation from ground roll data—the
517 role of higher modes, in 79th EAGE Conference and Exhibition.
- 518 4. Bergamo P, Dashwood B, Uhlemann S, Swift Chambers JE, Gunn DA, Donohue S (2016) Time-lapse
519 monitoring of fluid-induced geophysical property variations within an unstable earthwork using P-wave
520 refraction. *Geophysics* 81(4):17–27
- 521 5. Bièvre, G., Lacroix, P., Oxarango, L., Goutaland, D., Monnot, G., Fargier, Y., 2017. Integration of
522 geotechnical and geophysical techniques for the characterization of a small earth-filled canal dyke and
523 the localization of water leakage. *J. Appl. Geophys.* 139, 1–15.
- 524 6. Boore, D., 2007, Dave Boore's notes on Poisson's ratio (the relation between VP and VS),
525 http://www.daveboore.com/daves_notes.html, accessed 03 March 2017.
- 526 7. Busato, L., Boaga, J., Peruzzo, L., Himi, M., Cola, S., Bersan, S., Cassiani, G., 2016. Combined
527 geophysical surveys for the characterization of a reconstructed river embankment. *Eng. Geol.* 211, 74–
528 84.
- 529 8. Chao C et al (2006) Integrated geophysical techniques in detecting hidden dangers in river
530 embankments. *J Environ Eng Geophys* 11:83–94.
- 531 9. Colombero, C., Comina, C., Socco, L.V. (2019) Imaging near-surface sharp lateral variations with
532 surface-wave methods - Part 1: Detection and location, *Geophysics*, 84 (6), pp. EN93-EN111.
- 533 10. Comina C., Vagnon F., Arato A., Fantini F. and Naldi M., Application of a new electric streamer to the
534 characterization of river embankments, submitted to *Journal of Geotechnical and Geoenvironmental*
535 *engineering*.
- 536 11. Dal Moro G., M. Pipan, E. Forte and I. Finetti, 2005, Determination of Rayleigh wave dispersion curves
537 for near surface applications in unconsolidated sediments, SEG Technical Program Expanded Abstracts
538 2003, pages 1247-1250.
- 539 12. Foti, S., Lai, C.G., Rix, G.J., Strobbia, C., 2014. *Surface Wave Methods for Near-Surface Site*
540 *Characterization*. CRC Press.
- 541 13. Goff, D.S., Lorenzo, J.M., Hayashi, K. "Resistivity and shear wave velocity as a predictive tool of
542 sediment type in coastal levee foundation soils, 28th Symposium on the Application of Geophysics to
543 Engineering and environmental Problems 2015, SAGEEP 2015, pp. 145-154.
- 544 14. Hu Hao, Mustafa Senkaya, Yingcai Zheng, A novel measurement of the surface wave dispersion with
545 high and adjustable resolution: Multi-channel nonlinear signal comparison, *Journal of Applied*
546 *Geophysics*, Volume 160, 2019, Pages 236-241.
- 547 ~~14-15.~~ Karl, L., Fechner, T., Schevenels, M., François, S., Degrande, G., 2011. Geotechnical
548 characterization of a river dyke by surface waves. *Surf. Geophys.* 9, 515–527.
- 549 ~~15-16.~~ Khosro Anjom, F., D. Teodor, C. Comina, R. Brossier, J. Virieux, and L. V. Socco, 2019, Full
550 waveform matching of Vp and Vs models from surface waves, *Geophysical Journal International*, 218,
551 1873-1891.
- 552 ~~16-17.~~ Kramer S.L. 1996. *Geotechnical Earthquake Engineering*. Prentice Hall.
- 553 ~~17-18.~~ Kuras, O., Meldrum, P.I., Beamish, D., Ogilvy, R.D., Lala, D. "Capacitive resistivity imaging with
554 towed arrays", 2007, *Journal of Environmental and Engineering Geophysics*, 12 (3), pp. 267-279.
- 555 19. Lane Jr. J.W., Ivanov J., Day-Lewis F.D., Clemens D., Patev R. and Miller R.D. 2008. Levee evaluation
556 using MASW: Preliminary findings from the Citrus Lakefront Levee, New Orleans, Louisiana. 21st

557 Symposium on the Application of Geophysics to Engineering and Environmental Problems,
558 Philadelphia, USA, Expanded Abstracts, 703–712.

559 ~~18-20.~~ Li Jing, Zongcai Feng, Gerard Schuster, Wave-equation dispersion inversion, Geophysical Journal
560 International, Volume 208, Issue 3, 1 March 2017, Pages 1567–1578.

561 ~~19-21.~~ Lorenzo, J.M., Goff, D.S., Hayashi, K. "Soil-Type estimation beneath a coastal protection levee,
562 using resistivity and shear wave velocity" 22nd European Meeting of Environmental and Engineering
563 Geophysics, Near Surface Geoscience 2016.

564 ~~20-22.~~ Lutz K., Fechner T., Schevenels M., Stijn F. and Degrande G., 2011, Geotechnical characterization
565 of a river dyke by surface waves, Near Surface Geophysics, Volume9, Issue6, Pages 515-527.

566 ~~21-23.~~ Min D.-J. and Kim H.-S. 2006. Feasibility of the surface-wave method for the assessment of physical
567 properties of a dam using numerical analysis. Journal of Applied Geophysics 59, 236–243.

568 ~~24.~~ Pageot, D., Le Feuvre, M., Donatienne, L., Philippe, C., Yann, C., 2016. Importance of a 3D forward
569 modeling tool for surface wave analysis methods, in: EGU General Assembly Conference Abstracts. p.
570 11812.

571 ~~22-25.~~ Pan Yudi, Lingli Gao, Renat Shigapov, Multi-objective waveform inversion of shallow seismic
572 wavefields, Geophysical Journal International, Volume 220, Issue 3, March 2020, Pages 1619–1631.

573 ~~23-26.~~ Park, C. B., Xia, J., and Miller, R. D., 1998, Imaging dispersion curves of surface waves on
574 multichannel record: 68th Ann. Internat. Mtg., Soc. Explor. Geophys., Expanded Abstracts, 1377-1380.

575 ~~24-27.~~ Rahimi S., Clinton M. Wood, Folaseye Coker, Timothy Moody, Michelle Bernhardt-Barry, Behdad
576 Mofarraj Kouchaki, 2018, The combined use of MASW and resistivity surveys for levee assessment: A
577 case study of the Melvin Price Reach of the Wood River Levee, Engineering Geology, Volume 241,
578 Pages 11-24.

579 ~~25-28.~~ Samui, P., Sitharam, T.G. Correlation between SPT, CPT and MASW (2010) International Journal
580 of Geotechnical Engineering, 4 (2), pp. 279-288.

581 ~~26-29.~~ Samyn, K., Mathieu, F., Bitri, A., Nachbaur, A., Closset, L., 2014. Integrated geophysical approach
582 in assessing karst presence and sinkhole susceptibility along flood-protection dykes of the Loire River,
583 Orléans, France. Eng. Geol. 183, 170–184.

584 ~~27-30.~~ Sentenac P, Benes V, Keenan H (2018) Reservoir assessment using ~~invasive~~ geophysical
585 techniques. Environmental Earth Sciences 77(293):1-14

586 ~~28-31.~~ Socco, L.V. and Boiero, D., 2008. Improved Monte Carlo inversion of surface wave data, Geophys.
587 Prospect., 56, 357–371.

588 ~~29-32.~~ Socco, L. V., D. Boiero, S. Foti, and R. Wisén, 2009, Laterally constrained inversion of ground roll
589 from seismic reflection records: Geophysics, 74, no. 6, G35–G45.

590 ~~30-33.~~ Socco, L. V., and C. Comina, 2015, Approximate direct estimate of S-wave velocity model from
591 surface wave dispersion curves: 21st Annual International Conference and Exhibition, EAGE, Extended
592 Abstracts, A09.

593 ~~31-34.~~ Socco, L.V., Comina, C. and Khosro Anjom, F., 2017. Time-average velocity estimation through
594 surface-wave analysis: Part 1—S-wave velocity, Geophysics, 82(3), U49–U59.

595 ~~32-35.~~ Socco, L.V. and Comina, C., 2017. Time-average velocity estimation through surface-wave analysis:
596 Part 2—P-wave velocity, Geophysics, 82(3), U61–U73.

597 ~~33-36.~~ Takahashi T, Yamamoto T (2010) An attempt at soil profiling on a river embankment using
598 geophysical data. Explor Geophys 41(1):102–108

599 ~~34-37.~~ Takahashi, T., Aizawa, T., Murata, K., Nishio, H., Mat-suoka, T. "Soil permeability profiling on a
600 river embankment using integrated geophysical data", 2014, SEG Technical Program Expanded
601 Abstracts, 33, pp. 4534-4538.

602 ~~35-38.~~ Teodor D., Comina C., Khosro Anjom F., Socco L.V., Brossier R. and Virieux J., 2020, Challenges
603 in shallow targets reconstruction by 3D elastic full-waveform inversion – Which initial model?,
604 submitted to Geophysics.

Article Highlights:

- Effective V_s and V_p information are extracted from surface waves streamer data;
- An automated procedure for the seismic characterization of river embankments was developed;
- The procedure is demonstrated comparable to standard seismic processing approaches;
- Advantages in survey time and efficiency is highlighted.

1 **Effective Vs and Vp characterization from Surface Waves streamer** 2 **data along river embankments.**

3

4 Comina C.¹, Vagnon F.¹, Arato A.², Antonietti A.²5 ¹Dipartimento di Scienze della Terra, Università degli studi di Torino, Torino (IT)6 ²Techgea S.r.l., Torino (IT).

7

8

9 **ABSTRACT**

10

11 River embankments are linearly extended earth structures built for river flood protection. Their
12 continuity and uniformity are fundamental prerequisites to ensure and maintain their protection
13 efficiency. Weakness points usually develop in localized areas where geotechnical variability is
14 present in the embankment body or in the underlying subsoil. Given their significant length, and the
15 localized nature of weakness points, the characterization of river embankments cannot therefore
16 rely on local geotechnical investigations but requires the application of efficient and economically
17 affordable methods, able to investigate relevant lengths in a profitable way. This is even more
18 essential when the investigations are conducted near, or in foresee of, significant flood events, when
19 timing of the surveys is essential. In this paper the application of a procedure (W/D procedure) for
20 the seismic characterization of river embankments, specifically designed for surface waves streamer
21 data, is presented. The W/D procedure allows the combined definition of 2D shear (Vs) and
22 compressional (Vp) wave velocity models and can be developed in order to be automated as a fast
23 imaging tool. Its application to the characterization of a test site (Bormida river embankment,
24 Piedmont Region, Italy) is presented. It is also shown that the obtained results are comparable to
25 standard seismic processing approaches with the advantage of reduced survey time and increased
26 efficiency, giving preliminary results directly in the field.

27

28 **Article Highlights:**

- 29 • Effective Vs and Vp information are extracted from surface waves streamer data;
- 30 • An automated procedure for the seismic characterization of river embankments was
31 developed;
- 32 • The procedure is demonstrated comparable to standard seismic processing approaches;
- 33 • Advantages in survey time and efficiency is highlighted.

34

35 **Keywords:** surface waves, seismic characterization, river embankments.36 **Corresponding author:** Cesare Comina, cesare.comina@unito.it

37

38 **1. INTRODUCTION**

39 River embankments are linearly extended earth structures constructed to serve as flood control
40 systems during large rain events. A proper characterization of the embankment body is essential to
41 verify its uniformity and to monitor the occurrence of possible integrity losses which could
42 undermine its stability. In recent years, frequency and magnitude of extreme flood events have been
43 rapidly increasing in Central America, Southern Europe, and in Italy because of climate change.
44 Moreover, the poor maintenance of hydraulic structures, mostly reaching their design service life,
45 makes the adoption of specific interventions of paramount international relevance.

46 Given the significant length extension of these structures, and the localized nature of weakness
47 points, the characterization cannot rely only on local geotechnical investigations but requires the
48 application of efficient and economically affordable methods, able to investigate the whole
49 embankments in a profitable way. Moreover, geotechnical investigations usually require invasive
50 procedures (such as boreholes, penetration tests, etc) that are both expensive and time-consuming.
51 With this respect non-invasive, rapid and cost-effective methods are desirable to identify higher
52 potential hazard zones.

53 Among the available non-invasive geophysical methods (Chao et al., 2006; Bergamo et al., 2016;
54 Takahashi et al., 2014; Sentenac et al., 2018), the seismic ones have peculiar advantages for the soil
55 characterization. Seismic velocities, and particularly shear wave velocity (V_s), are directly related
56 to the dynamic stiffness of the material, which is an important mechanical parameter for the
57 recognition of soil layers. Moreover, in the field of geotechnical engineering, huge research effort
58 has been spent on the correlation of V_s to parameters obtained from standard geotechnical tests. Site
59 specific and general correlations exist to porosity, plasticity index, to the shear modulus at higher
60 strains and to standard geotechnical in situ tests such as cone penetration, standard penetration and
61 dilatometer tests (e.g. Kramer, 1996; Samui, 2010; Foti et al., 20014).

62 Among the seismic methods the multichannel analysis of surface waves (MASW), based on the
63 Rayleigh wave dispersion curve (DC) analysis, is considered the most effective for the
64 determination of V_s profiles. This method can be efficiently applied to seismic streamer data
65 dragged along embankments and overall linear earth structures. This allows the determination of
66 several V_s profiles to offer an almost 2D representation of the velocity field. Several literature
67 applications of this methodology are available along embankments, river dykes and earth dams (e.g.
68 Lutz et al., 2011; Lane et al., 2008; Min and Kim, 2006). Eventually, MASW surveys can be used
69 in combination with geoelectrical and geotechnical methods to allow for more complete
70 characterization (e.g. Samyn et al., 2014; Busato et al., 2016; Bièvre et al., 2017; Rahimi et al.,
71 2018; Arato et al. 2020).

72 The main limitations of this methodology are related to the high non-linearity of the DC inversion
73 procedure and to the lack of compressional wave velocity (V_p) information. Several global
74 inversion approaches have been proposed for the DC inversion (e.g. [Socco and Boiero, 2008](#)), with
75 the aim of tackling the problem of non-uniqueness of the solution. More elaborated inversion
76 strategies for reconstructing 2D shear wave velocity sections including waveform information (e.g.
77 wave-equation dispersion inversion (WD), [Li et al., 2017](#), or multi-objective waveform inversion
78 (MOWI), [Pan et al., 2020](#)) have been also proposed. Nevertheless, all these approaches are highly
79 time consuming, particularly for increasing number of DCs to be analysed, and can be adopted only
80 in the post-processing stage, not allowing for an effective in situ characterization. The lack of V_p
81 information can also be a disadvantage since V_p is known to be correlated with saturation levels
82 and related Poisson ratio of the materials. This last could be indeed an important parameter to be
83 determined along river embankments, to complete the characterization.

84 To overcome these limitations, the application of a new procedure ([Socco et al., 2017](#); [Socco and](#)
85 [Comina, 2017](#)) for the analysis of Rayleigh wave fundamental mode DC is adopted in this paper.
86 This procedure is based on the relationship between Rayleigh wave wavelength and investigation
87 depth (W/D procedure) and exploit the higher sensitivity of the DCs to time-average shear wave
88 velocity ($V_{s,z}$) than to layered velocity profiles and the sensitivity of the Rayleigh wave skin depth
89 to V_p . The W/D procedure allows the determination of both 2D V_s and V_p sections from the DCs
90 using a direct data transform approach. The relationship between the wavelength of the Rayleigh
91 wave fundamental mode and the investigation depth (W/D relationship) is estimated through a
92 reference V_s and $V_{s,z}$ profile and used to directly transform all DCs into V_s profiles. The sensitivity
93 of the W/D relationship to Poisson ratio is moreover exploited to obtain also V_p profiles along the
94 studied embankment. The procedure has already demonstrated its reliability both on synthetic and
95 real data, producing V_s and V_p models which allow a reliable waveform matching in comparison to
96 benchmarks ([Khosro Anjom et al., 2019](#)) and effective full waveform inversion starting models
97 ([Teodor et al., 2020](#)).

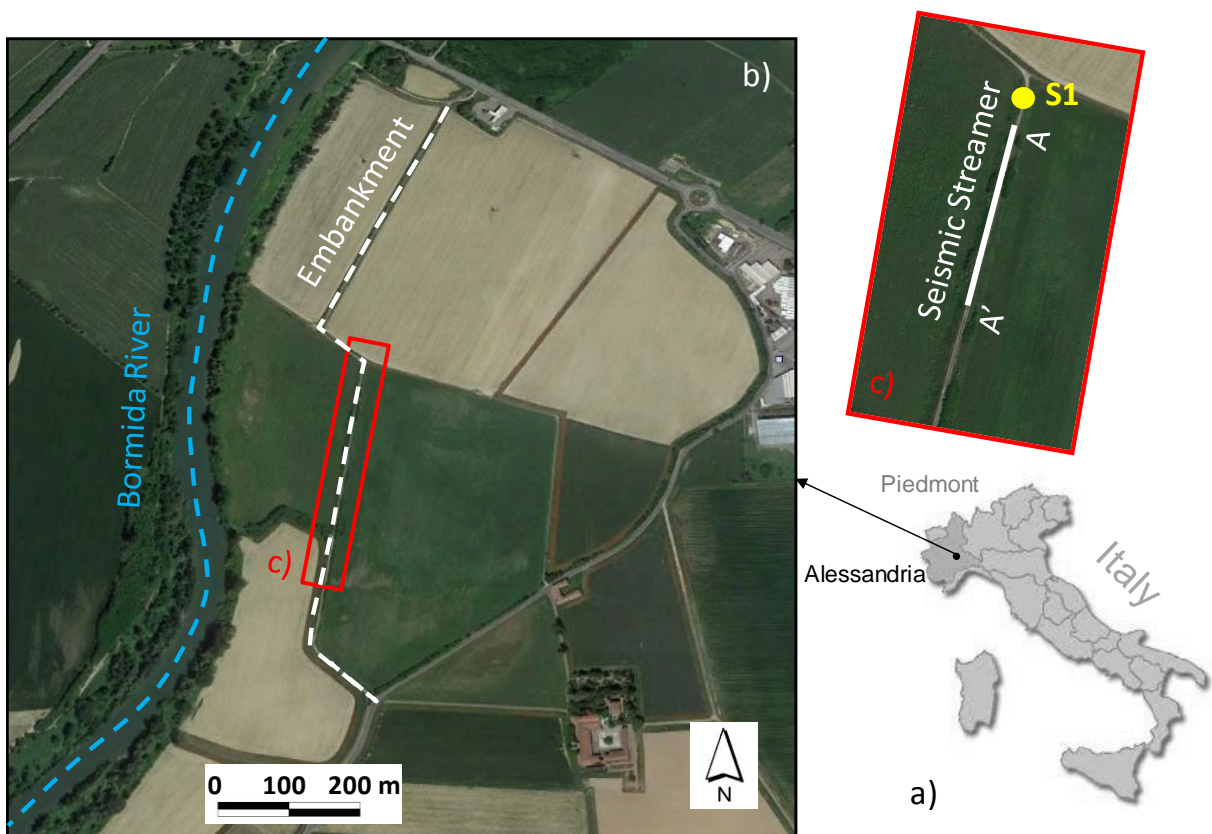
98 Another significant advantage of the proposed W/D procedure is that, being a data transform
99 approach, it does not have particular computational requirements. In principle, it could therefore be
100 applied also during in situ measurement campaigns for a fast imaging of the seismic properties of
101 the studied embankment. This products a strong reduction of survey time and increased efficiency.
102 In this paper, the procedure is specifically implemented for surface waves streamer data and its
103 application to the characterization of a test site (Bormida river embankment, Piedmont Region,
104 Italy) is presented. It is shown that the obtained results are comparable to standard seismic

105 processing approaches with the advantage of reduced survey time and increased efficiency, and that
106 preliminary results can be obtained directly during in situ measurements.

107

108 2. TEST SITE AND EXECUTED SURVEYS

109 The test site investigated in this paper is the right embankment of the Bormida river, east of the city
110 of Alessandria, in Spinetta Marengo municipality, Piedmont Region, NW Italy (Figure 1). The
111 embankment is separated from the river by the presence of a 200 m wide floodplain that serves as
112 expansion area during floods (Figure 1). The top of the embankment rises about 9 m from the free
113 surface of the river, and about 3 m from the floodplain. The soil composition of the embankment
114 (embankment body and foundation) was obtained by available geotechnical tests: a borehole,
115 executed on the top of the embankment in correspondence of an embankment curve (S1, in Figure 1
116 inlet) and a dynamic penetration super heavy test (DPSH) executed in the proximity of the borehole.
117 Both the borehole and DPSH interested embankment body and foundation soil till about 16 m
118 depth.



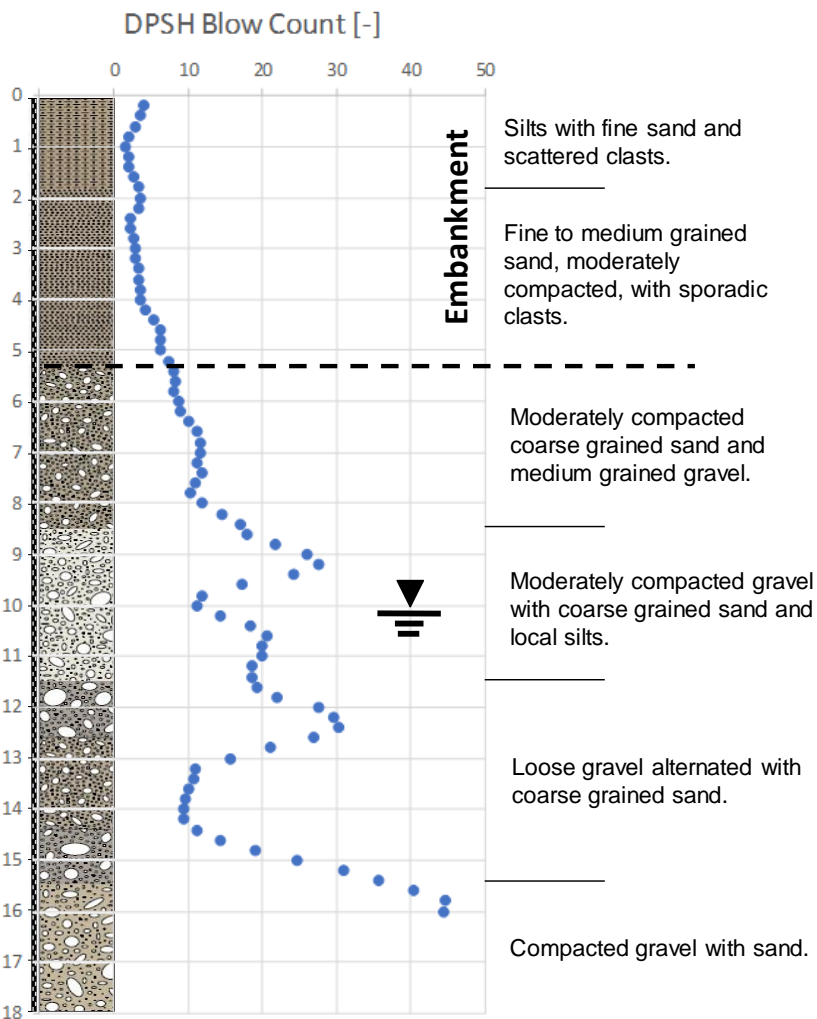
119

120 **Figure 1 – Location of the test site: a) north western Italian Po plain, Piedmont region, near the city of**
121 **Alessandria, b) detail of the studied embankment and c) executed surveys.**

122 The geotechnical setting (Figure 2) can be synthesized as constituted by silts with fine sands and
123 scattered clasts changing to fine to medium grained sands, moderately compacted, with sporadic

124 clasts, up to about 5.3 m depth (embankment body) overlaying a coarse sand and gravel formation
 125 moderately to medium compacted with intercalated silts and local compaction reduction with depth.
 126 At the moment of execution of the borehole (November 2007) the water table was reported at about
 127 10 m depth from the embankment top; given the height of the river, the water table is therefore
 128 supposed to be fed by the river and its elevation strictly dependent on the water level within the
 129 river.

130 As it can be observed in the stratigraphic log, the transition from embankment body to natural
 131 subsoil does not appear to be particularly sharp. This can be an indication that the construction
 132 procedure did not involved relevant reworking of the first subsoil and that lateral differences in
 133 depth and nature of this contact could be present along the embankment. Taking as reference the
 134 DPSH result, local eventual differences along the embankment body will be investigated using
 135 seismic streamer data dragged along a specific portion of the embankment (Figure 1).



136

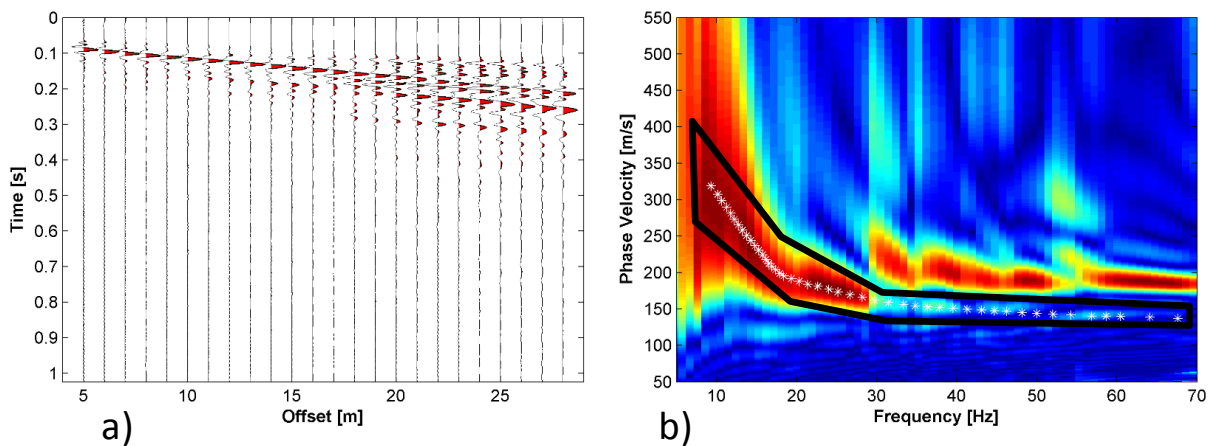
137 **Figure 2 – Stratigraphic log and geotechnical description of the encountered formations with evidence**
 138 **of the DPSH results.**

139 An embankment sector of about 90 m, south with respect to the S1 borehole (Figure 1), was
140 investigated in May 2019 with a seismic land streamer constituted of 24, 4.5 Hz vertical geophones
141 mounted on coupling sliders at 1 m spacing. The streamer was dragged by a pick-up truck and was
142 moved along the studied reach at 2 m steps; for each moving step a single seismic shot was
143 registered. The seismic source was a 40 kg accelerated mass mounted on the pick-up back; a 5 m
144 source offset was adopted in the acquisitions. The streamer was connected to a DaQLink IV
145 (Seismic Source, 2016) acquisition device on the pick-up truck, storing the data in a survey laptop
146 and eventually applying pre-processing steps. Seismograms were acquired with a 0.5 ms sampling
147 interval, -50 ms pretrig and 1.024 s total recording length. A total of 45 seismograms were therefore
148 acquired during the survey. On these data several processing steps were applied for the definition of
149 2D Vs and Vp models with the proposed W/D procedure.

150

151 3. METHODOLOGY

152 An example seismic shot is reported in Figure 3a. The used source and streamer setup allowed the
153 acquisition of high-quality data, with clear evidence of surface waves dispersive pattern and also
154 particularly evident first arrivals of compressional waves.



155

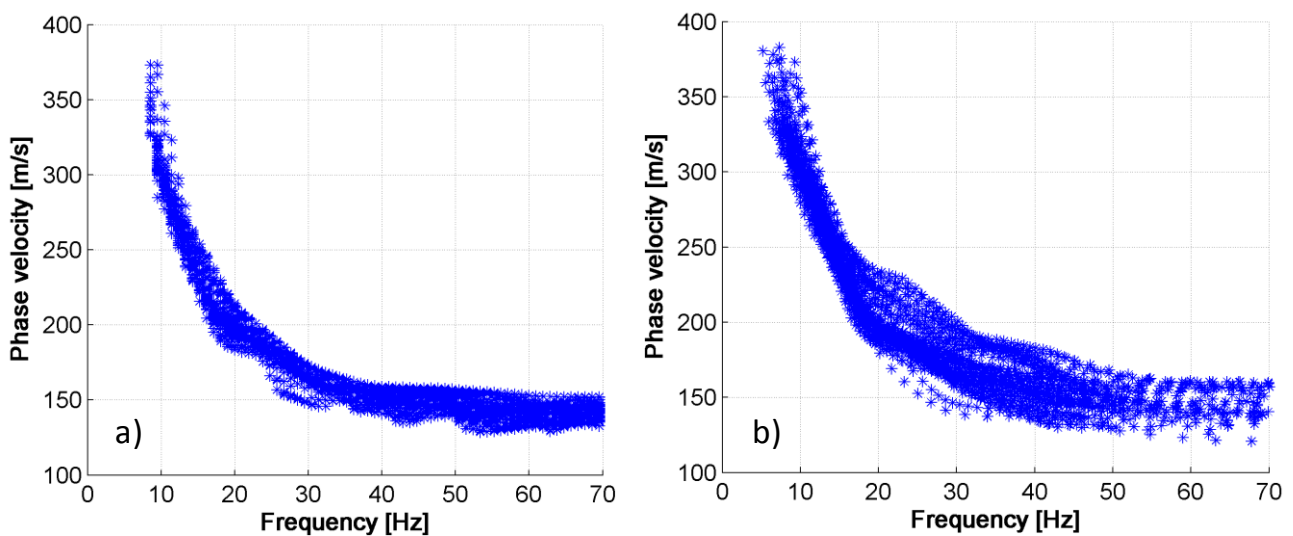
156 **Figure 3 – Data processing procedures on acquired seismograms: a) example seismic shot, b)**
157 **dispersion curve extraction with evidence of the applied mask (black line) and selected high energy**
158 **maxima (white asterisks).**

159 DCs extraction was performed with two different procedures: first, the dispersion image for each
160 seismogram was obtained by means of a phase-shift approach (Park et al., 1998) implemented in
161 MATLAB® routines. The phase-shift approach has demonstrated to maintain very good
162 performances even when a limited number of traces is considered (Dal Moro et al., 2005).
163 Alternatively, to further improve the accuracy of dispersion measurement, a multi-channel

164 nonlinear signal comparison (MNLSC, Hu et al., 2019) can be adopted, producing high and
165 adjustable resolution among a wide detected frequency range.

166 On the dispersion image the zone pertinent to the fundamental mode propagation was selected with
167 a mask (black line in Figure 3b) and energy maxima were automatically searched within this area
168 (white asterisks in Figure 3b). The mask selected for the first shot can be either automatically used
169 for all the following shots (automatic procedure) or partially adjusted to follow eventual variations
170 in the energy distribution (semi-automatic procedure). In the first case a rough, but fully automated,
171 DCs selection is obtained, in the second case a more refined, but more time consuming, analysis is
172 allowed, to better evidence eventual lateral variations. On both these selected DC groups eventual
173 smoothing and manual outlier removal can be applied to obtain more continuous and reliable
174 curves.

175 In Figure 4 the resulting DCs selected for all the shots from automatic and semi-automatic
176 procedures are reported. For some of the shots a transition of the absolute energy maxima towards
177 higher modes was observed in the high-frequency range (e.g. frequencies higher than 30Hz in
178 Figure 3b). Nevertheless the fundamental mode can still be followed as local maxima thank to the
179 adopted mask that allowed to isolate the correct portion of the dispersion image to be considered,
180 excluding the higher modes from the maxima searching. It can be evidenced that the DC ranges are
181 very similar with corresponding velocity transition. Nevertheless, the semi-automatic procedure
182 (Figure 4b) shows higher variability for the medium-high frequency range (shallower layers) as a
183 result of the application of a variable mask. Most of the results reported in the paper refer to the
184 DCs selected with this approach. In the discussion section some comparisons are however presented
185 with the results obtainable with the automatic procedure also.



186

187 **Figure 4 – DCs selected for all the shots: a) automatic procedure and b) semi-automatic procedure.**

188 The application of the W/D procedure to the extracted DCs requires the knowledge of a single V_s
189 and $V_{s,z}$ reference profile along the seismic line together with its associated DC. This profile can be
190 either extracted from the data themselves, by performing the inversion of a representative DC
191 among the ones extracted, or it can be obtained by independent seismic or geotechnical data.

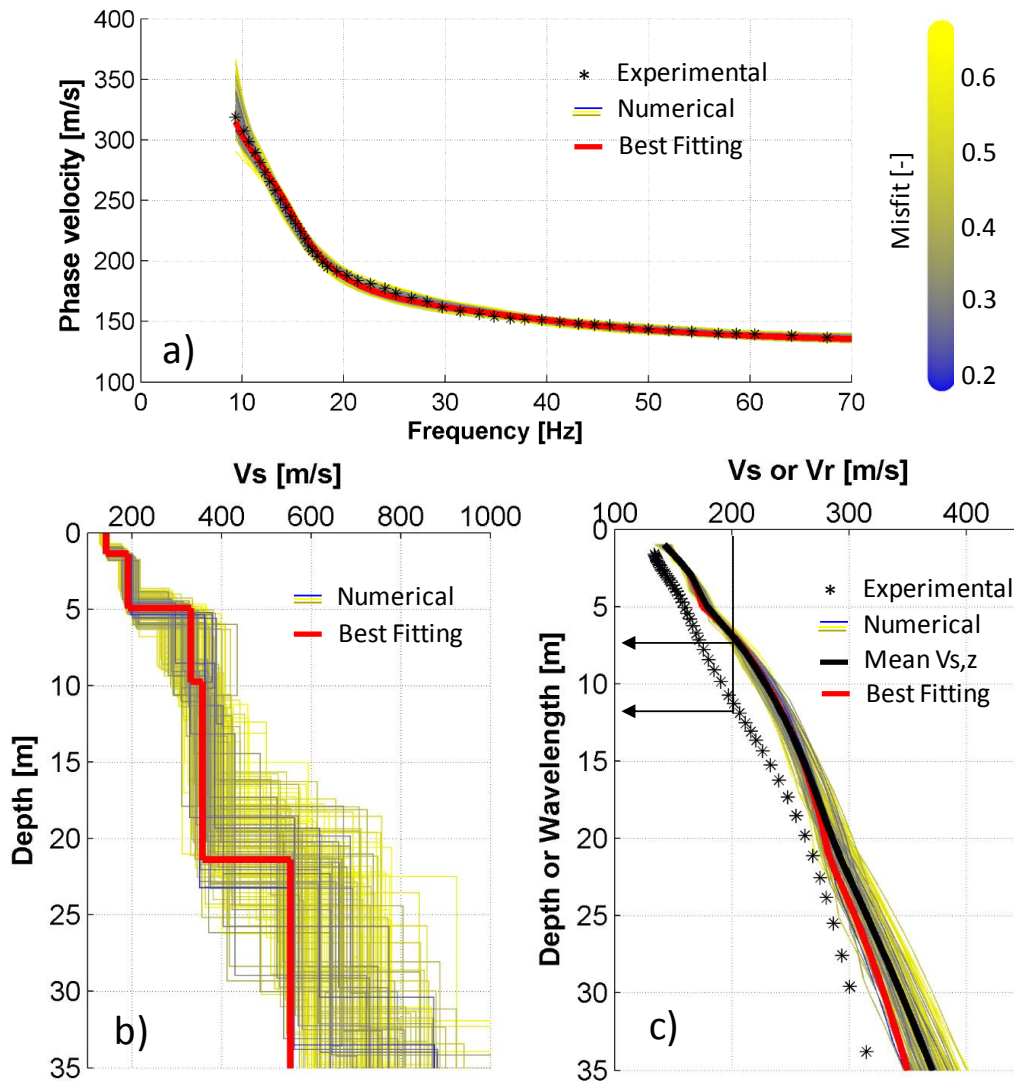
192 In this paper the first method was adopted using a Monte Carlo Inversion (MCI) algorithm (Socco
193 and Boiero, 2008) which efficiently limits potential non-uniqueness of the solution and results in
194 reliable V_s and $V_{s,z}$ profiles. The inversion implies the definition of a wide model space by
195 selecting ranges for each model parameter (V_s , thicknesses and the Poisson ratio of each layer) and
196 performing random sampling (10^5 profiles) among these ranges. Please note that, in order to allow
197 for the W/D procedure to be applied, also Poisson ratio of each layer is considered as a model
198 parameter, contrary to what usually performed in the inversion of DC curves.

199 Example application of the inversion process to the DC reported in Figure 3b, which was selected
200 as reference, is reported in Figure 5. It can be observed that the set of statistical equivalent profiles
201 selected from the MCI assess the presence of a contrast at the bottom of the embankment around 5
202 m depth (Figure 5b). This set of profiles, and their correspondent numerical DCs, is represented in
203 Figure 5 with a relative misfit representation based on the absolute difference between each profile
204 misfit and the best fitting one (in red in Figure 5).

205 It can also be noted that the higher variability in terms of V_s profiles (Figure 5b) strongly reduces
206 when the time average shear wave velocity is considered ($V_{s,z}$, in Figure 5c). With this respect the
207 best selected profile (in red in Figure 5c) and the mean of the statistical set (in black in Figure 5c)
208 almost superimpose for the top portion of the profile. Socco and Comina (2015) have already shown
209 that the non-uniqueness of the DC inversion very slightly affects the estimation of time-average
210 velocity, and hence, the $V_{s,z}$ obtained from inverted profiles is very robust. Nevertheless, given the
211 increased uncertainty at the bottom of the profile, the following analyses were limited to 20 m
212 depth, which is enough for investigating both the embankment and a significant portion of the
213 foundation subsoil at the studied test site.

214 Using the reference V_s and $V_{s,z}$ profiles and all the extracted DCs, the proposed data transform
215 procedure is then applied as following: i) the estimated $V_{s,z}$ and its corresponding DC are used to
216 compute the reference W/D relationship; ii) the reference W/D relationship is used to transform all
217 DCs into $V_{s,z}$ models; iii) an apparent Poisson ratio is estimated using the reference W/D
218 relationship and the reference V_s model; iv) using the apparent Poisson ratio, each $V_{s,z}$ profile is
219 transformed into a $V_{p,z}$ profile; v) all the reconstructed $V_{s,z}$ and $V_{p,z}$ profiles are transformed into
220 V_s and V_p profiles with an interval velocity analysis.

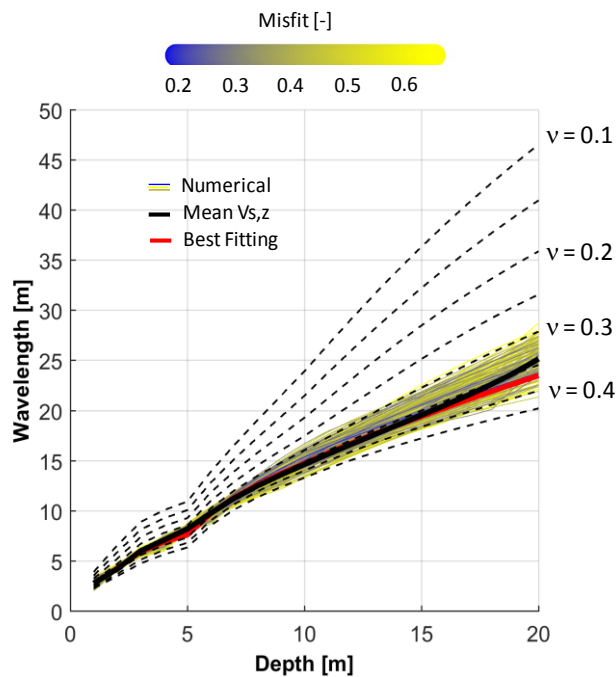
221



222

223 **Figure 5 – MCI of the reference DC curve: a) experimental and numerical dispersion curves b) best**
 224 **fitting profile and set of statistically equivalent profiles and c) experimental dispersion curve as a**
 225 **function of wavelength, time average velocities of best fitting profile and statistically equivalent**
 226 **profiles with their mean.**

227 Steps i) and iii) of the procedure require more explanations. The meaning of the W/D relationship is
 228 represented in [Figure 5c](#): for each $V_{s,z}$ value, the wavelength (W) at which the phase velocity (V_r)
 229 of the DC is equal to the $V_{s,z}$ (see the arrows in [Figure 5c](#)) is searched for each depth (D). With all
 230 the W/D pairs at which $V_{s,z}$ and phase velocity are equal a relationship is obtained (W/D
 231 relationship). This relationship is represented in [Figure 6](#) for the best fitting profile (in red), for the
 232 mean of the statistically equivalent profiles (in black) and for all the statistically equivalent profiles.
 233 Consistency of the extracted W/D relationships is evidenced.



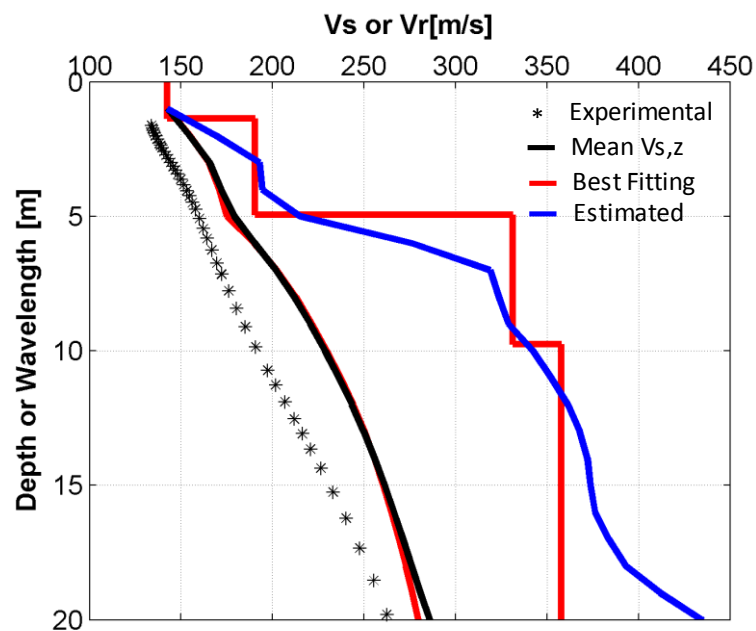
234

235 **Figure 6 – The W/D relationship for the reference DC for the best fitting profile (in red), for the mean**
 236 **of the statistically equivalent profiles (in black) and for all the statistically equivalent profiles**
 237 **compared with the ones obtained with different Poisson ratio values. Reference Poisson ratio values**
 238 **are indicated on the right of the plot.**

239 This relationship represents the surface waves' skin depth for increasing wavelengths and has been
 240 demonstrated (Socco and Comina, 2017) to be influenced by the Poisson ratio of the formation.
 241 With the reference V_s and $V_{s,z}$ profiles it is therefore possible to build different synthetic W/D
 242 relationships by changing the value of the Poisson ratio (ν) of the layers (assumed constant for all
 243 the layers). These synthetic W/D relationships are reported in Figure 6 (dashed black lines) for
 244 some example values of the Poisson ratio. It can be noted that Poisson ratio acts on the slope of
 245 W/D relationship. In particular, the slope decreases when Poisson ratio increases. Therefore the
 246 slope of the experimentally determined W/D relationship contains information on the actual Poisson
 247 ratio of the formation. The actual apparent Poisson ratio profile of the formation can be therefore
 248 searched by associating to each depth the value of Poisson ratio that corresponds to the linear
 249 interpolation between the upper and lower nearest synthetic W/D relationships. In this way an
 250 apparent Poisson ratio profile with depth can be obtained for the reference DC. This profile can be
 251 later used to transform all the $V_{s,z}$ profiles into $V_{p,z}$ profiles allowing for a 2D V_p section to be
 252 later computed.

253 An example application of the W/D procedure to the reference DC is reported in Figure 7. It can be
 254 observed that the $V_{s,z}$ of the best fitting profile (continuous red line in Figure 7) and the mean $V_{s,z}$
 255 of the statistical set (continuous black line in Figure 7) almost superimpose for the first 20 m depth.

256 It can be also noted that the W/D procedure allows the estimate of a V_s model (in blue in Figure 7)
 257 very near to the best fitting one (layered red line in Figure 7) obtained from the MCI of the DC. The
 258 model obtained with this procedure has also the advantage of not making any assumption with
 259 respect to the number of layers of the profile. For this reason, it can result smoother with respect to
 260 the layered profile but also more correspondent to the actual geotechnical situation below the
 261 embankment. Particularly, it can be observed that the transition from embankment body to bottom
 262 layers with this estimated profile appear to be more correspondent to what evidenced in the DPSH
 263 results (Figure 2) with respect to the sharp interface evidenced by the MCI result.



264
 265 **Figure 7 – Application of the W/D procedure to the reference DC for V_s profile determination and**
 266 **comparison with the best fitting result (both in term of layered velocity model and $V_{s,z}$) from MCI.**

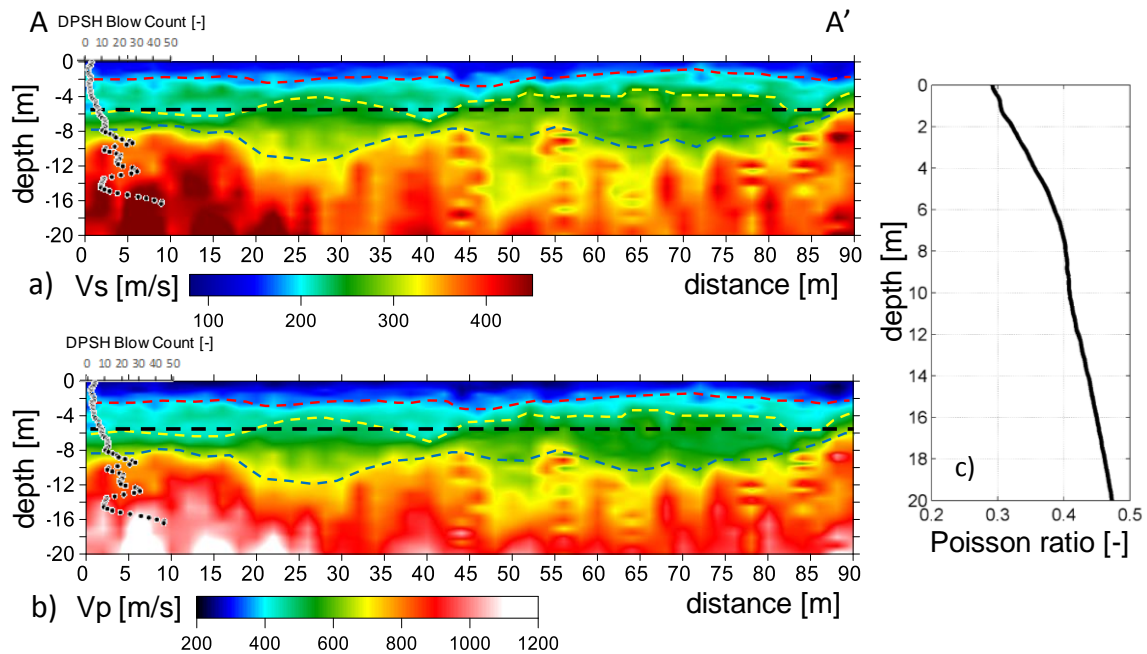
267 All the V_s and V_p profiles estimated with the W/D procedure are then interpolated along the studied
 268 embankment to allow for a 2D visualization of the V_s and V_p velocities distributions. The data
 269 gridding was performed in Surfer (Golden software) with an interpolation grid of 2 m in the
 270 horizontal direction (equal to the acquisition step) and of 0.5 m in the vertical direction.

271 To validate the velocity models obtained with the application of the W/D procedure the obtained
 272 results are benchmarked against standard seismic processing approaches. For V_s , all the dispersion
 273 curves extracted were inverted with a laterally constrained inversion (LCI) approach (Auken and
 274 Christiansen, 2004; Socco et al., 2009). For this inversion, the same number of layers of the MCI
 275 was assumed. For V_p , processing was carried out by picking the first breaks on each acquired
 276 seismogram, picked first breaks were then interpreted in tomographic approach with the use of the
 277 software Rayfract (Intelligent Resources Softwares Inc.).

278

4. RESULTS

279 Results of the application of the W/D procedure are reported in Figure 8. Particularly, the V_p result
280 is obtained from the V_s one with the application of the apparent Poisson ratio obtained from the
281 W/D procedure. This last is assumed constant through the whole profile and therefore the resulting
282 V_p velocity field is a transformation of the V_s one with similar properties. Both V_s and V_p sections
283 can discriminate the transition from the shallow silts and sands to the bottom gravels along the
284 embankment and delineate the embankment bottom. Coherently with the borehole results and
285 geotechnical tests this transition falls, on the left side of the sections, where the surveys are nearer
286 to the geotechnical tests (the DPSH Blow Count profile is also reported in Figure 8a and b), around
287 5.3 m depth.



288

289 **Figure 8 – Results of the application of the W/D procedure to extracted DCs (section A-A’): a) V_s**
290 **section, b) V_p section and c) resulting Poisson ratio. On both the sections the supposed depth of the**
291 **embankment is also reported (dashed black line) together with coloured dashed lines, derived by the**
292 **velocity models, indicating the transition between the shallow silts and sands (in red), the thickness of**
293 **the embankment (in yellow) and the transition to compacted gravels and sands (in blue). The DPSH**
294 **Blow Count profile is also reported at the beginning of the sections.**

295 However, along the embankment a variation of the depth of this interface can be evidenced.
296 Particularly, localized anomalies appear in the V_s section suggesting an increase in the depth of the
297 shallow silts and sands of the embankment (yellow dashed line in Figure 8) around 40 m
298 progressive distance. Conversely, the depth of the interface appears to be shallower in the
299 progressive distance range between about 50 to 80 m.

300 Seismic surveys are also able to depict the transition (red dashed line in [Figure 8](#)) from silts with
301 fine sands and scattered clasts to fine to medium grained sands, as reported from the borehole and
302 DPSH results, within the embankment. A deeper increase in velocity is also observed around 8 m
303 depth on the left side of [Figure 8](#), were the transition to more compacted gravels (blue dashed line
304 in [Figure 8](#)) is evidenced by borehole and DPSH results . This more compacted formation appears
305 however to increase its depth along the section moving away from the borehole and showing on
306 average lower velocity values. Localized velocity inversions are also partially observable below 8 m
307 in the leftmost portions of the Vs section. This evidence again well compares with what reported by
308 the DPSH results.

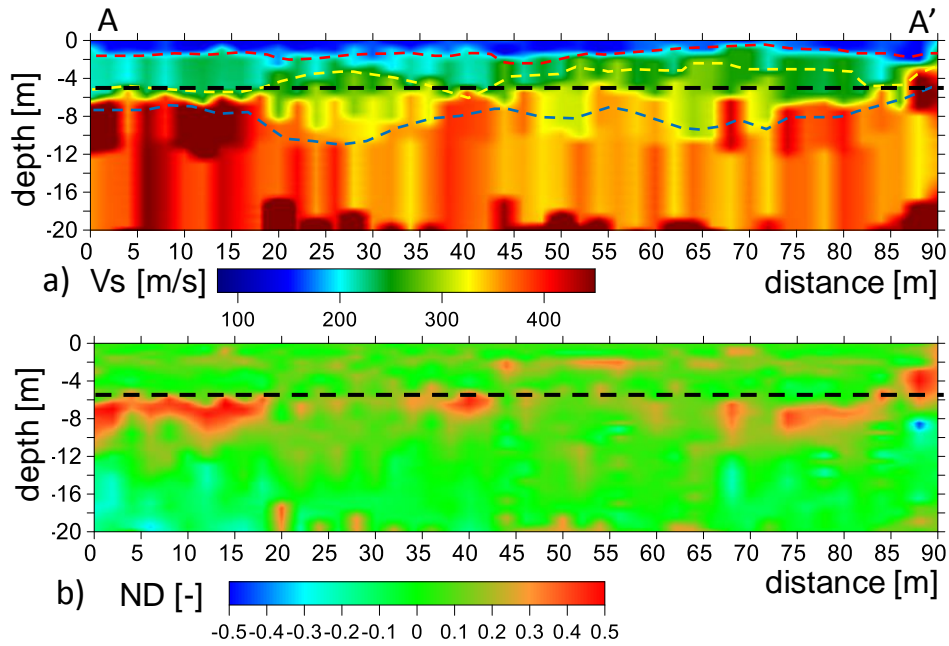
309 Notwithstanding the information on the position of the water table at the site (around 10 m) the
310 range of Vp velocities extracted by the procedure does not report, for increasing depths, velocity
311 ranges usually attributed to saturated materials (i.e. around 1400-1500 m/s). It must be underlined
312 that the time span between the two surveys is relevant (from November 2007 to May 2019) so that
313 eventual variations on the water table depth could be present. Nevertheless, the Poisson ratio profile
314 extracted with the W/D procedure ([Figure 8c](#)) shows a marked increase nearly around 10 m
315 exceeding the 0.4 value and tending to 0.5. Poisson ratio of saturated soils is usually reported to be
316 in this range ([Boore, 2007](#)). It must be underlined that the Poisson ratio profile here presented is the
317 interval Poisson ratio obtained through the Vp/Vs ratio of the resulting models. This is different
318 from the apparent Poisson ratio that is estimated in the W/D procedure ([Figure 6](#)) for the DC
319 transformation.

320 Results of the LCI processing of the extracted dispersion curves are reported in [Figure 9a](#). A good
321 convergence of the inversion was obtained with LCI resulting in a final RMS error of 1.7%.

322 The comparison of the LCI result with the W/D procedure is performed in [Figure 9b](#) in term of
323 normalized differences, taking as reference the LCI results, with the formula:

$$324 \quad ND = \frac{V_{i,LCI} - V_{i,W/D}}{V_{i,LCI}} \quad (1)$$

325
326 were $V_{i,W/D}$ is the velocity value obtained from the W/D procedure and $V_{i,LCI}$ is the velocity value
327 obtained from the LCI in each location within the models. Therefore, positive values of the
328 normalized difference indicate zones where the W/D procedure underestimate the velocity, negative
329 values indicate the opposite. To allow computing the normalized differences in each point of the
330 models also layered LCI results were gridded with the same interpolation scheme of the W/D
331 procedure results.



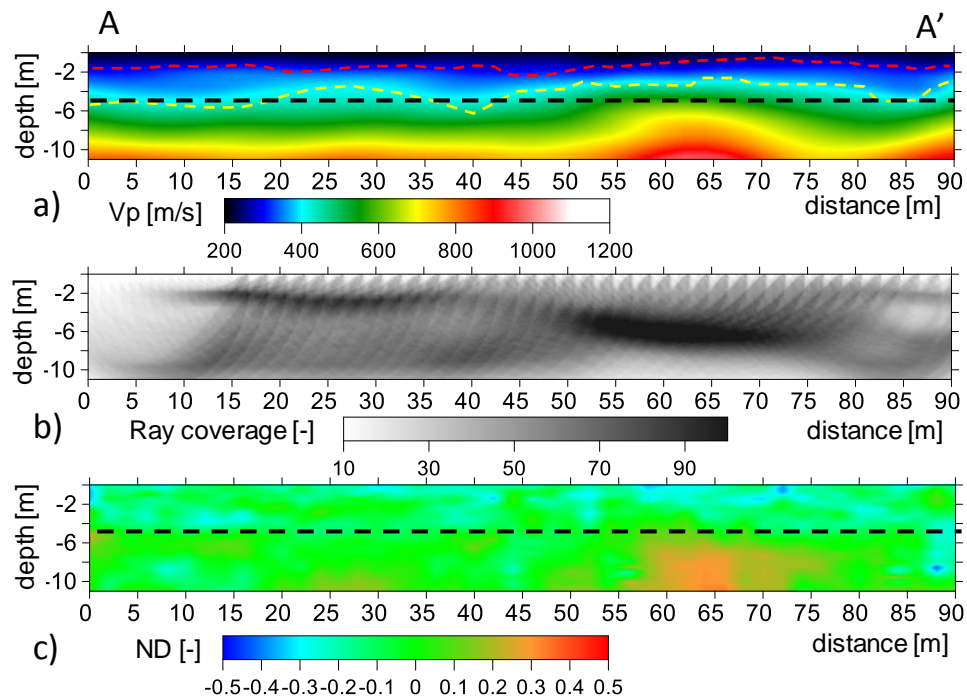
332

333 **Figure 9 – Results of the LCI of the extracted DCs (section A-A’): a) Vs section and b) Normalized**
 334 **differences with the Vs results of the W/D procedure. On both the sections the supposed depth of the**
 335 **embankment is also reported (dashed black line). Over the LCI section, the interfaces evidenced by the**
 336 **W/D procedure indicating the transition between the shallow silts and sands (in red), the thickness of**
 337 **the embankment (in yellow) and the transition to compacted gravels and sands (in blue), are**
 338 **superimposed.**

339 **Figure 9** shows that the Vs velocity range obtained using LCI inversion is comparable with that
 340 from the W/D procedure. The interfaces evidenced by the W/D procedure are reported for
 341 comparison over the resulting Vs image. Similar variability in the depth of the interfaces is noted.
 342 As an example, both the increased depth of shallower silts and sands around progressive 40 m and
 343 the shallower depth of the embankment in the progressive distance range between about 50 to 80 m
 344 are confirmed. Most of the normalized differences among the W/D and LCI models fall within a
 345 $\pm 10\%$ range indicating the good correspondence of the two results. The only portions of the section
 346 affected by higher positive normalized differences cannot be attributed to errors in the W/D
 347 procedure, but to the layering assumption in the LCI. The layered discretization adopted in the LCI
 348 can indeed result in an overestimation of the velocity near the layer boundaries (see also **Figure 7**
 349 for comparison). Most of the higher difference values fall indeed near the embankment/foundation
 350 soil interface where the layered profile results from LCI tend to give a sharper transition than the
 351 W/D result.

352 Results of the tomographic inversion of picked first arrivals are reported in **Figure 10** and
 353 compared, in term of normalized differences, with the Vp results obtained with the W/D procedure.
 354 The same equation 1 was adopted for the computation of normalized differences with Vp values

355 from W/D procedure and first arrivals tomography (these last substituting the LCI values in
356 equation 1).



357

358 **Figure 10 – Results of the first break tomography (section A-A’): a) Vp section, b) Ray coverage along**
359 **the section and c) Normalized differences with the Vp results of the W/D procedure. On both the**
360 **sections the supposed depth of the embankment is also reported (dashed black line). Over the**
361 **tomography the first two interfaces evidenced by the W/D procedure, indicating the transition**
362 **between the shallow silts and sands (in red), the thickness of the embankment (in yellow), are**
363 **superimposed.**

364 From Figure 10 it can be observed that, given the reduced length of the streamer adopted, the depth
365 of investigation of the tomography is limited to about 10 m, or even less in some portions.
366 Nevertheless, within this depth, a high ray coverage is obtained in most of the section by the
367 combined elaboration of all the shots. A good convergence of the inversion was obtained with a
368 resulting RMS error of 2.7% after the final iteration.

369 Again, from Figure 10 it can be observed that the tomographic inversion depicts the same velocity
370 range compared to the one obtained with the W/D procedure. Given the reduced investigation depth
371 of the tomography only the first two interfaces evidenced by the W/D procedure are reported for
372 comparison over the resulting Vp image. Similar variability in the depth of these two interfaces is
373 noted. As an example, both the increased depth of shallower silts and sands around progressive 40
374 m and the shallower depth of the embankment in the progressive distance range between about 50
375 to 80 m are confirmed. Being based on relatively long-path raytracing, the tomographic result

376 shows generally a reduced lateral resolution in the identification of the velocity variations within the
377 section.

378 Most of the normalized differences, also for V_p , fall within a $\pm 10\%$ range indicating the good
379 correspondence of the two results. The only portion of the section showing higher normalized
380 differences can be attributed to a lower ray coverage zone (see [Figure 10b](#) below 7 m at about 55 to
381 70 progressive distances) making the assumed V_p values less reliable in the tomography. Given its
382 shallower investigation depth, also the tomography does not highlight a marked increase of V_p
383 values, at the bottom of the model, attributable to the presence of the water table.

384

385 **5. DISCUSSION**

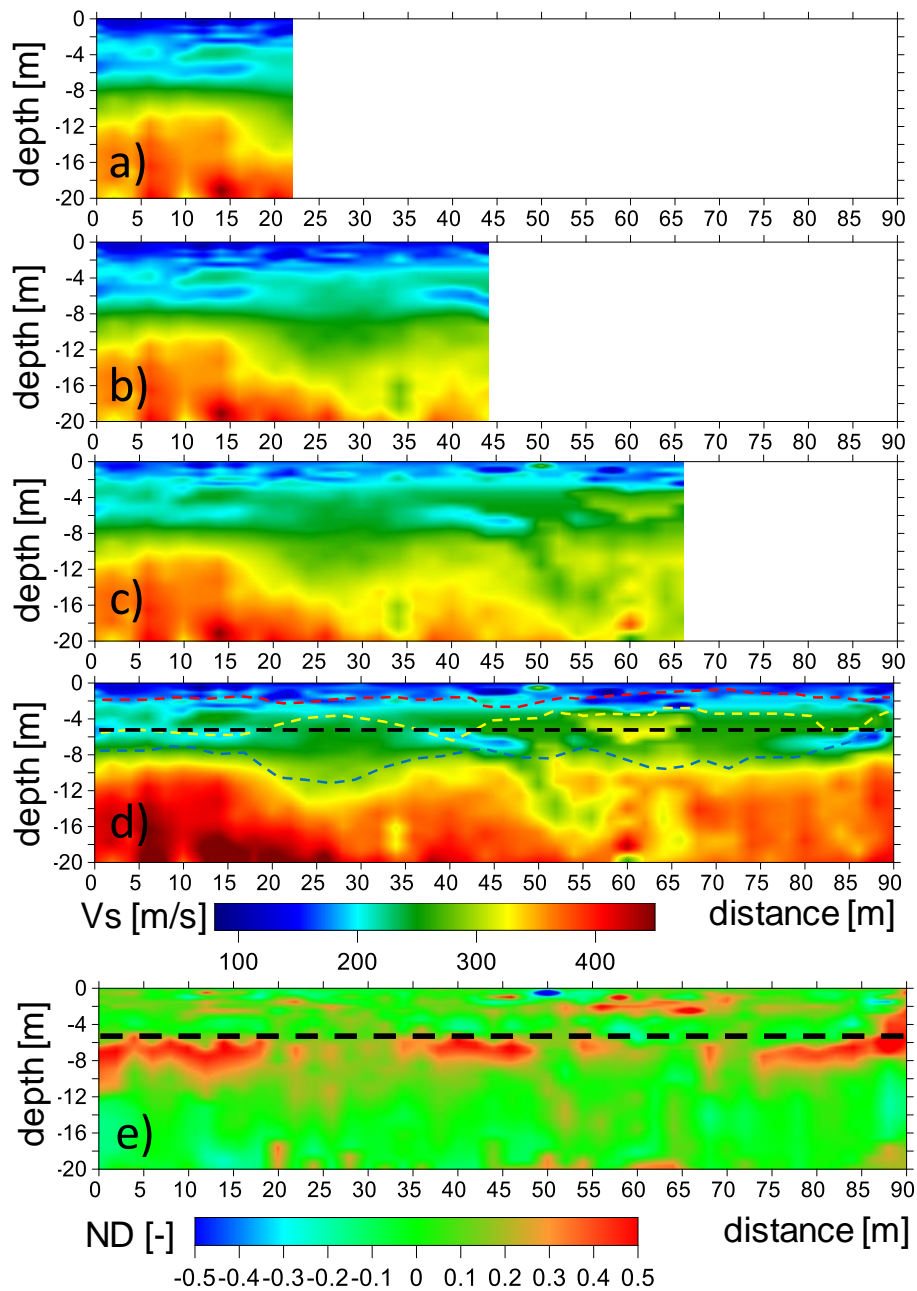
386 It was shown in the paper that the results obtainable with the W/D procedure are comparable both in
387 terms of V_s and V_p to standard seismic processing approaches. This comparison validates therefore
388 the application of the W/D procedure. It was observed, in the presented case study, that most of the
389 normalized differences between the W/D procedure and both LCI and first arrivals tomography fall
390 within a $\pm 10\%$ range, indicating the good correspondence of the two results. Higher normalized
391 differences along the sections can be attributed to different resolution or underlying
392 methodological assumptions among the methods and cannot be considered as an error in the W/D
393 procedure. Therefore, the W/D procedure can be established as a reliable alternative to the methods
394 here compared for the characterization of embankments and overall linear earth structures.

395 The W/D procedure has also main advantages with respect to usually seismic processing
396 approaches applied to the data obtained from similar surveys: i) being a data transform approach it
397 does not requires relevant processing and time consuming interpretations; ii) it does not make any
398 assumption with respect to the number of layers present along the investigated embankment and iii)
399 allow the combined estimation of V_s and V_p for increased depths given the same acquisition setup.

400 Particularly the first advantage is important if the speed of the surveys is considered, for example in
401 situations in which a fast and preliminary evaluation of the state of health of an embankment is
402 required. This can be the case of surveys conducted after, or in foresee of, significant rain and/or
403 flood events. In these conditions the W/D procedure, applied to the fully automated extracted DCs
404 ([Figure 4a](#)), can allow for a first, almost immediate, on site evaluation of the V_s and V_p velocity
405 field. Both the automated DC extraction step and the conversion of DC data to V_s and V_p profiles is
406 indeed a very fast process (few tens of seconds on a notebook), that outputs direct velocity models
407 while the acquisition is in progress and the streamer is dragged along the embankment.

408 An example application of this direct visualization of the V_s section during data acquisition is
409 reported in [Figure 11](#). It can be particularly observed that the final V_s section determined from the

410 fully automated extracted DCs (Figure 11d) is roughly comparable with the one determined with the
 411 semi-automatic procedure (Figure 8a) with very similar depiction of the main interfaces.



412
 413 **Figure 11 – Example application of the direct visualization of the Vs section during data acquisition:**
 414 **a), b) and c) Vs sections while dragging the streamer along the embankment; d) final Vs section and c)**
 415 **Normalized differences with the LCI. In d) and e) the supposed depth of the embankment is also**
 416 **reported (dashed black line). In d) the interfaces evidenced by the semi-automated W/D procedure,**
 417 **indicating the transition between the shallow silts and sands (in red), the thickness of the embankment**
 418 **(in yellow) and the transition to compacted gravels and sands (in blue), are superimposed.**

419
 420 The presence of some artefacts can be however noted within the section and can be related to the
 421 reduced precision of the automatic picking of the DCs. A general increase in the normalized

422 differences with the LCI (Figure 11d) is also observed, with the presence of localized anomalous
423 local velocity values (e.g. see the shallow portion of the embankment around progressive 50 m).
424 Nevertheless, the general imaging of the Vs structure can be considered accurate enough for a first
425 estimation of the geotechnical variability at the site and a useful tool for a preliminary identification
426 of anomalous portions of the examined embankments. Given the use of the same Poisson ratio
427 profile (Figure 8c), uniform through the section, very similar considerations can be performed for
428 what concerns the resulting Vp image.

429 This direct visualization requires the knowledge of reference Vs and Vs,z profiles over which
430 calibrate the W/D relationship and the following Poisson ratio computation. In the present paper
431 these reference profiles were obtained through MCI of a reference DC. The same approach can be
432 adopted on site at the beginning of the surveys by selecting one of the clearer DCs during the first
433 shots. Nevertheless, the MCI step can be significantly time consuming and not always applied with
434 reliability on site. Possible alternative approaches would therefore require the execution of initial
435 detailed tests and interpretations through which determine with accuracy the reference profiles and
436 only later proceed with the execution of the streamer surveys. Alternatively, the reference profiles
437 can be extracted from already available geotechnical and/or geophysical surveys along the
438 embankment. With this respect the W/D procedure already showed comparable results also with
439 respect to Down Hole surveys (Socco et al., 2017).

440 Limitations of the proposed W/D procedure can be related to: i) its application to only fundamental
441 mode DC; ii) the assumption of a laterally invariable W/D relationship and Poisson ratio along the
442 embankment. With respect to the first one, the W/D procedure has been mainly developed and
443 applied to fundamental mode DC, but some attempts have been already made to include also higher
444 propagation modes (e.g. Bamarouf et al., 2017). Including higher modes showed to give advantages
445 mainly with respect to the investigation depth, even though it is a more time-consuming process.

446 However, this could be a necessary step along embankments with peculiar shape dimensions, since
447 it is well known that the shape of the embankment could influence the surface wave dispersive
448 pattern and modes superposition (e.g. Karl et al., 2011). Pageot et al. (2016) have also shown that
449 internal structure layering can emphasize geometrical effects and produce DCs very different from
450 the theoretical 1D case, for both the fundamental and higher modes. In these conditions even a
451 multi-modal inversion approach could encounter some limitations to infer accurate Vs and Vp
452 models.

453 These effects have not been particularly noted at the site. As it can be observed in Figure 3b, higher
454 modes are indeed present in the higher frequency range, but the fundamental mode propagation is
455 still easily recognizable as local energy maxima. This may be related to the reduced contrast

456 between the embankment body and the underlying subsoil (Figure 2) which limits the layering
457 effect and to the relevant width of the embankment (width to height ratio of about 5.5) which limits
458 the presence of 3D effects.

459 Conversely the laterally invariant assumption could be easily overcome using appropriate clustering
460 techniques on the extracted DCs that can be analysed for grouping them into subsets with
461 homogeneous properties. The W/D procedure has then to be applied to each of the identified
462 subsets. The application of this further processing step however increases again the computation
463 times and prevent a direct in situ application of the procedure but has been shown to provide
464 increased resolution in the identification of sharp lateral variations with the W/D procedure (Khosro
465 Anjom et al., 2019; Teodor et al., 2020).

466 The clustering approach was judged to be unnecessary in the presented case study given the
467 uniformity of the extracted DCs (see Figure 4) which suggest the presence of smooth depth
468 variations along the embankment but the absence of particularly sharp variations. When sharp
469 lateral variations along the embankment are the main survey target alternative identification
470 methods based on the surface waves spectral properties (e.g. Colombero et al., 2019) could also be
471 applied to the acquired streamer data.

472 To allow for a more complete characterization of the state of health of embankments, seismic data
473 are usually combined with electric resistivity data. These last can indeed give important information
474 on the variations of soil composition and water saturation, detect development of weak zones and
475 identify local anomalies potentially related to seepage. The combined use of seismic and electrical
476 data can indeed provide an effective geotechnical characterization of these earth structures, as
477 shown by several research groups that are working on their integration (e.g. Takahashi et al., 2014;
478 Goff et al. 2015; Lorenzo et al., 2016). In this respect the W/D procedure has its natural
479 development in combination with mobile electric systems allowing also a fast and effective
480 evaluation of resistivity properties (e.g. Kuras et al., 2007; Comina et al., 2020).

481 **6. CONCLUSION**

482 This paper presents the application of a novel processing approach (W/D procedure) to surface
483 wave streamer data. This approach is based on the definition a wavelength/depth (W/D) relationship
484 for surface waves and allows the combined definition of shear (V_s) and compressional (V_p) wave
485 velocities. The results obtained within the paper with the W/D procedure are comparable to
486 standard seismic processing approaches with the advantage of reduced survey time and increased
487 efficiency. It was shown in the paper as the W/D procedure can be developed in order to be
488 completely automated and used as a fast in situ imaging tool along embankments for preliminary
489 evaluations on their state of life.

490 Processing of the seismic streamer data yielded to an effective characterization of the V_s and V_p
491 velocity field along the studied embankment. The origin and properties of the anomalies
492 encountered could be better studied with the use of local geotechnical investigations to provide a
493 more specific knowledge on the state of life of the embankment. The produced seismic sections, if
494 properly calibrated with the few independent geotechnical tests available, can be nevertheless used
495 for preliminary stability evaluations also in portion of the embankment non directly covered by
496 geotechnical tests.

497 Further studies, already planned and partially executed, include the application of the W/D
498 procedure to different embankments shapes with the eventual inclusion of higher modes in the
499 interpretation. Moreover, the combined acquisition of electrical resistivity data, even with
500 innovative acquisition approaches, will allow the contemporary execution of resistivity and seismic
501 surveys with even more reduced survey time and increased knowledge on the state of health of the
502 embankments due to the acquisition of the different complementary parameters.

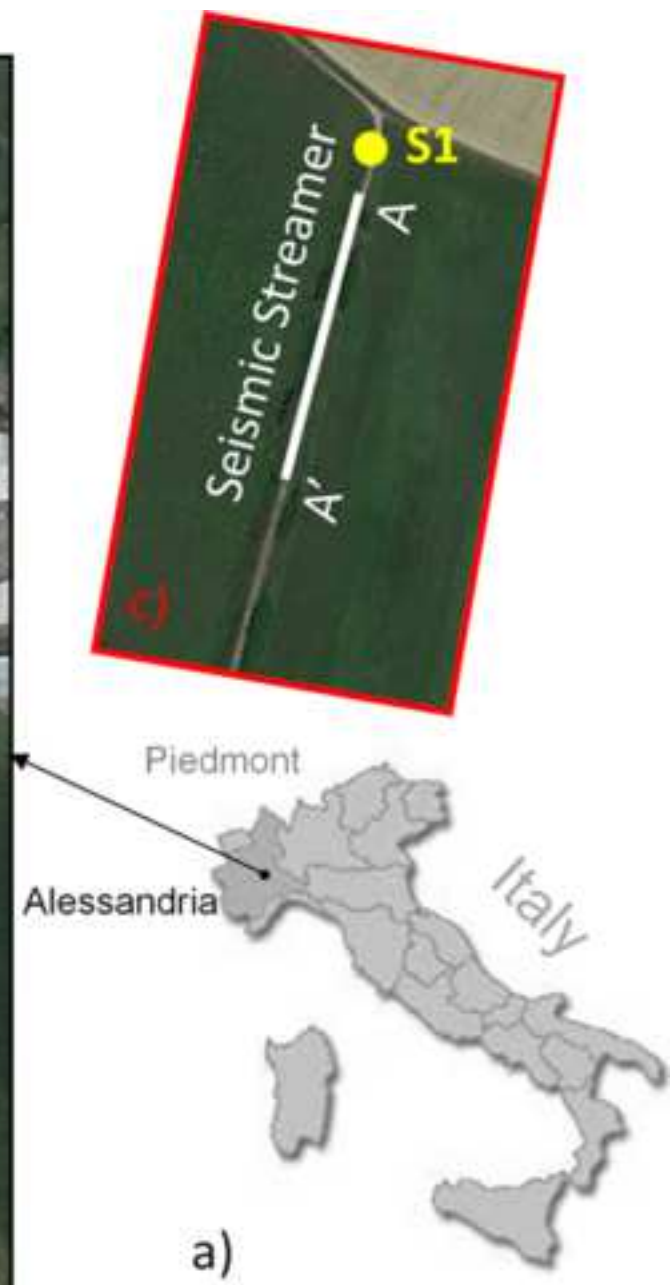
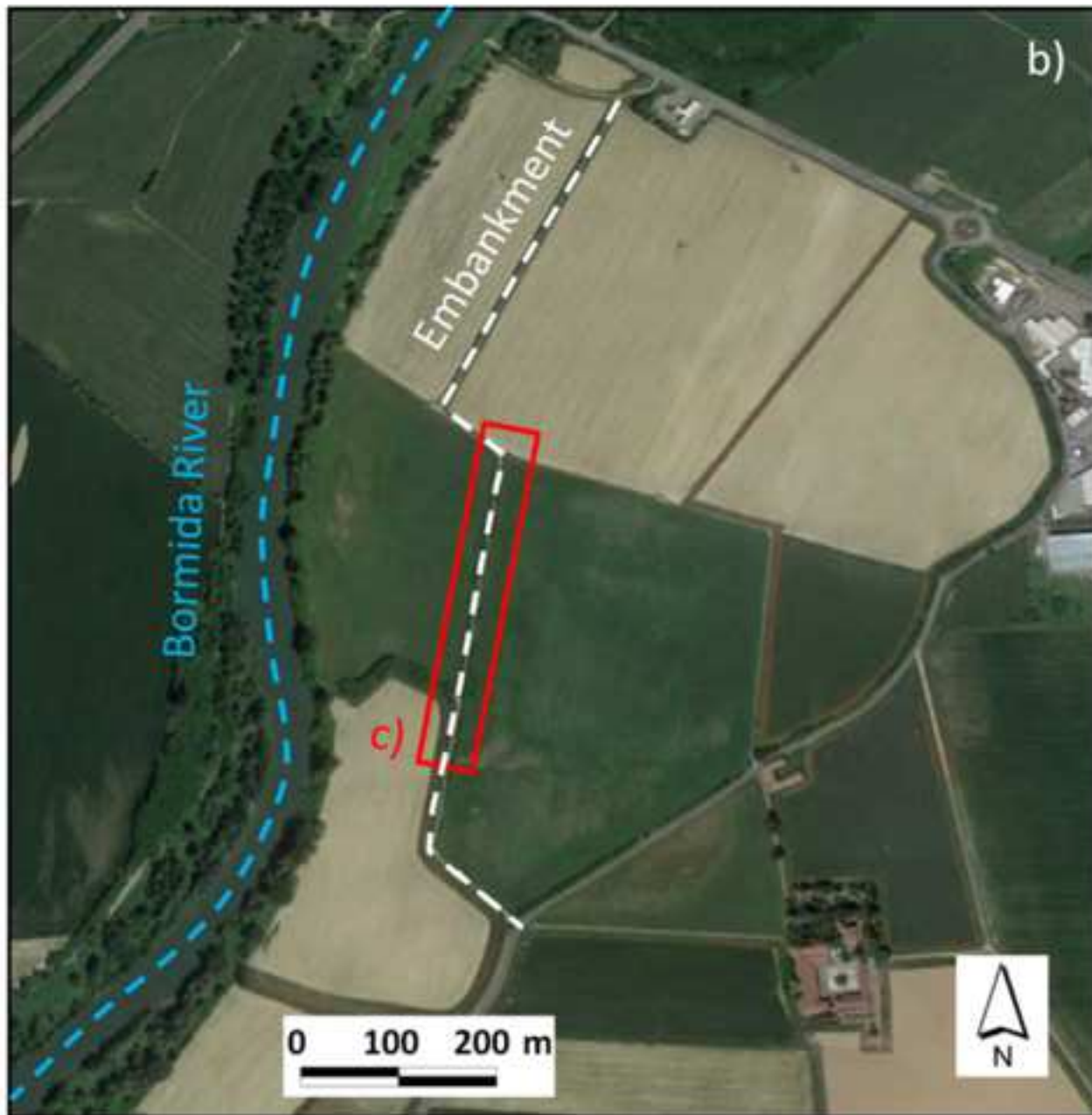
503 **ACKNOWLEDGMENTS**

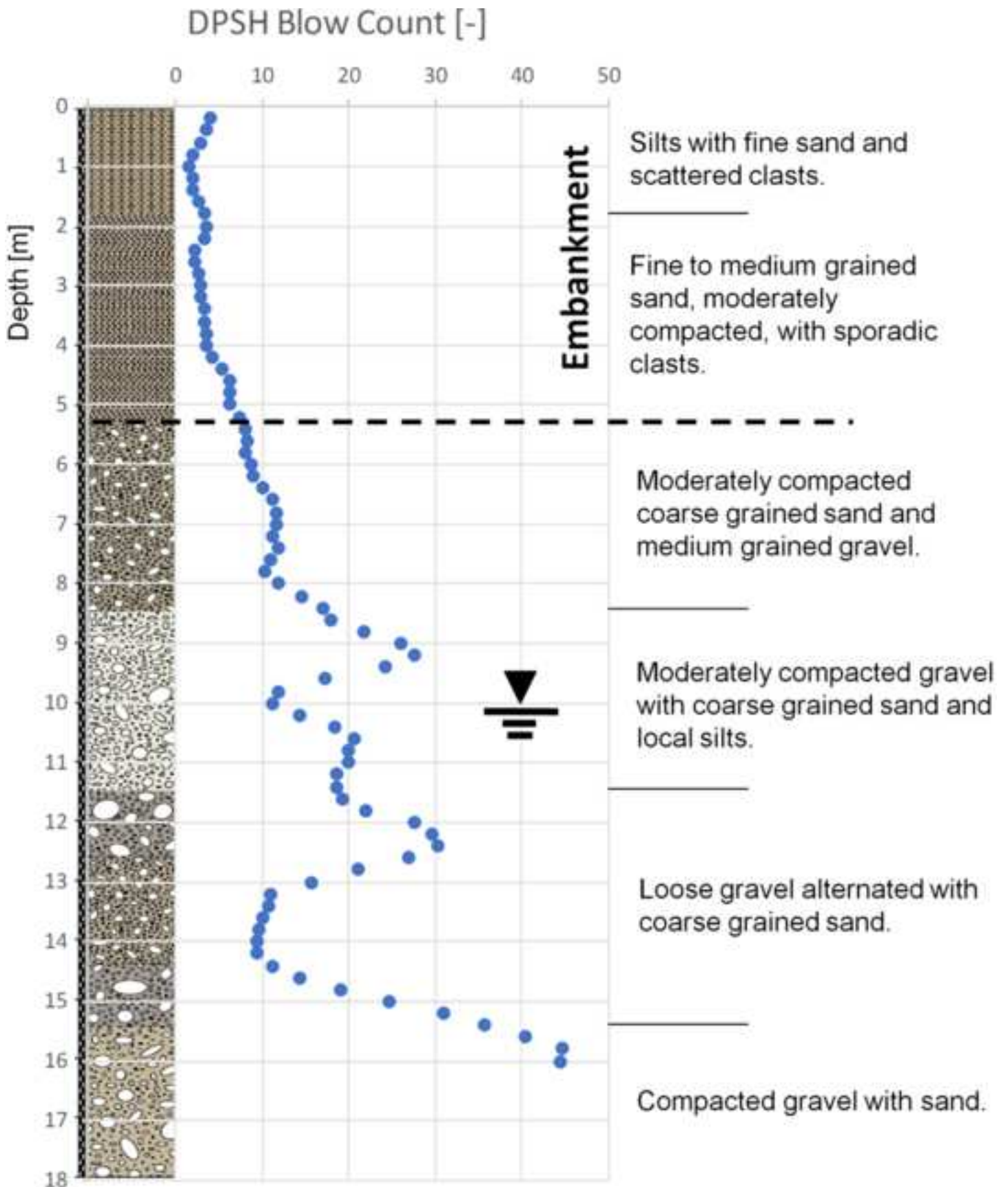
504 This work has been funded by FINPIEMONTE within the POR FESR 14/20 "Poli di Innovazione - Agenda
505 Strategica di Ricerca 2016 - Linea B" call for the project Mon.A.L.I.S.A. (313-67). Authors thank Daniele
506 Negri for helping during acquisition surveys.

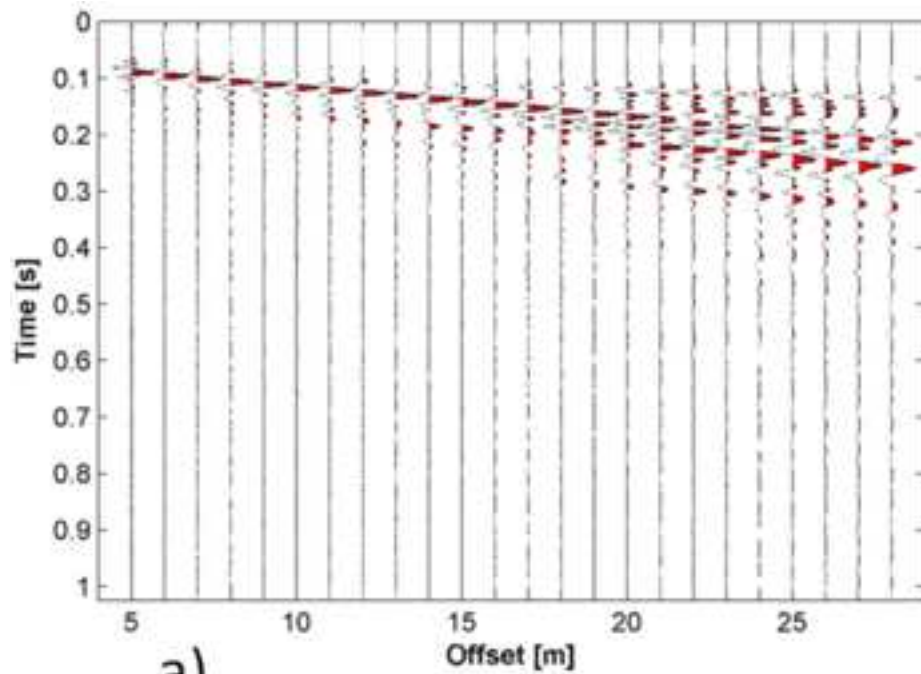
507 **REFERENCES**

- 508 1. Arato A., Naldi M., Vai L., Chiappone A., Vagnon F. and Comina C. (2020) Towards a Seismo-Electric
509 land streamer, submitted for the 6th International Conference on Geotechnical and Geophysical Site
510 Characterization, 7-11 September 2020, Budapest.
- 511 2. Auken, E., and A. V. Christiansen, 2004, Layered and laterally constrained 2D inversion of resistivity
512 data: *Geophysics*, 69, 752–761.
- 513 3. Bamarouf, T., Socco, L.V. & Comina, C., 2017. Direct Statics estimation from ground roll data—the
514 role of higher modes, in 79th EAGE Conference and Exhibition.
- 515 4. Bergamo P, Dashwood B, Uhlemann S, Swift Chambers JE, Gunn DA, Donohue S (2016) Time-lapse
516 monitoring of fluid-induced geophysical property variations within an unstable earthwork using P-wave
517 refraction. *Geophysics* 81(4):17–27
- 518 5. Bièvre, G., Lacroix, P., Oxarango, L., Goutaland, D., Monnot, G., Fargier, Y., 2017. Integration of
519 geotechnical and geophysical techniques for the characterization of a small earth-filled canal dyke and
520 the localization of water leakage. *J. Appl. Geophys.* 139, 1–15.
- 521 6. Boore, D., 2007, Dave Boore's notes on Poisson's ratio (the relation between VP and VS),
522 http://www.daveboore.com/daves_notes.html, accessed 03 March 2017.
- 523 7. Busato, L., Boaga, J., Peruzzo, L., Himi, M., Cola, S., Bersan, S., Cassiani, G., 2016. Combined
524 geophysical surveys for the characterization of a reconstructed river embankment. *Eng. Geol.* 211, 74–
525 84.
- 526 8. Chao C et al (2006) Integrated geophysical techniques in detecting hidden dangers in river
527 embankments. *J Environ Eng Geophys* 11:83–94.
- 528 9. Colombero, C., Comina, C., Socco, L.V. (2019) Imaging near-surface sharp lateral variations with
529 surface-wave methods - Part 1: Detection and location, *Geophysics*, 84 (6), pp. EN93-EN111.
- 530 10. Comina C., Vagnon F., Arato A., Fantini F. and Naldi M., Application of a new electric streamer to the
531 characterization of river embankments, submitted to *Journal of Geotechnical and Geoenvironmental*
532 *engineering*.
- 533 11. Dal Moro G., M. Pipan, E. Forte and I. Finetti, 2005, Determination of Rayleigh wave dispersion curves
534 for near surface applications in unconsolidated sediments, SEG Technical Program Expanded Abstracts
535 2003, pages 1247-1250.
- 536 12. Foti, S., Lai, C.G., Rix, G.J., Strobbia, C., 2014. *Surface Wave Methods for Near-Surface Site*
537 *Characterization*. CRC Press.
- 538 13. Goff, D.S., Lorenzo, J.M., Hayashi, K. "Resistivity and shear wave velocity as a predictive tool of
539 sediment type in coastal levee foundation soils, 28th Symposium on the Application of Geophysics to
540 Engineering and environmental Problems 2015, SAGEEP 2015, pp. 145-154.
- 541 14. Hu Hao, Mustafa Senkaya, Yingcai Zheng, A novel measurement of the surface wave dispersion with
542 high and adjustable resolution: Multi-channel nonlinear signal comparison, *Journal of Applied*
543 *Geophysics*, Volume 160, 2019, Pages 236-241.
- 544 15. Karl, L., Fechner, T., Schevenels, M., François, S., Degrande, G., 2011. Geotechnical characterization
545 of a river dyke by surface waves. *Surf. Geophys.* 9, 515–527.
- 546 16. Khosro Anjom, F., D. Teodor, C. Comina, R. Brossier, J. Virieux, and L. V. Socco, 2019, Full
547 waveform matching of Vp and Vs models from surface waves, *Geophysical Journal International*, 218,
548 1873-1891.
- 549 17. Kramer S.L. 1996. *Geotechnical Earthquake Engineering*. Prentice Hall.
- 550 18. Kuras, O., Meldrum, P.I., Beamish, D., Ogilvy, R.D., Lala, D. "Capacitive resistivity imaging with
551 towed arrays", 2007, *Journal of Environmental and Engineering Geophysics*, 12 (3), pp. 267-279.
- 552 19. Lane Jr. J.W., Ivanov J., Day-Lewis F.D., Clemens D., Patev R. and Miller R.D. 2008. Levee evaluation
553 using MASW: Preliminary findings from the Citrus Lakefront Levee, New Orleans, Louisiana. 21st

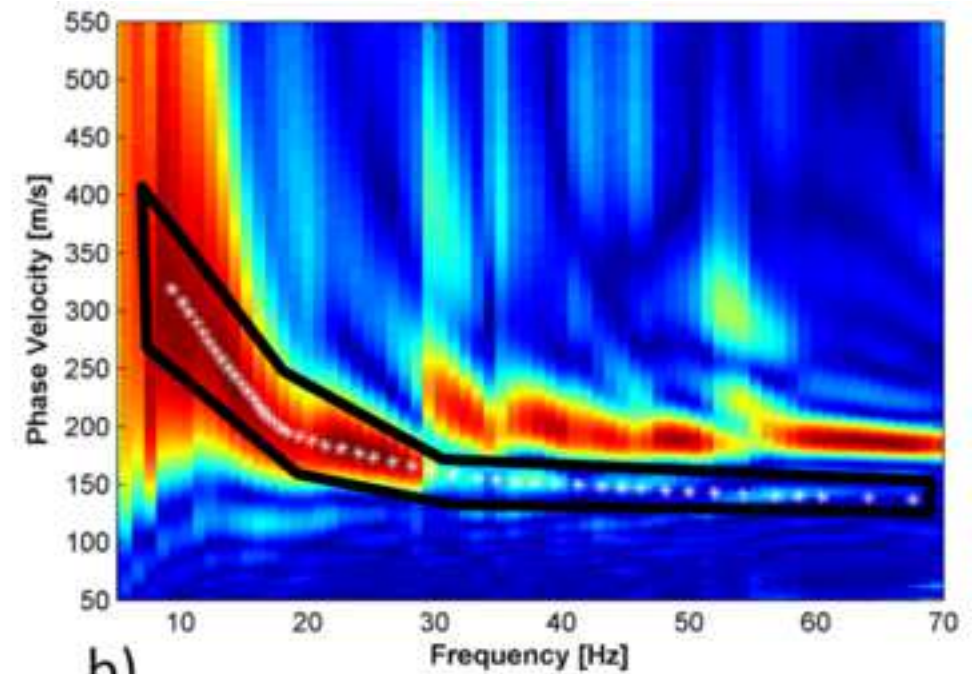
- 554 Symposium on the Application of Geophysics to Engineering and Environmental Problems,
555 Philadelphia, USA, Expanded Abstracts, 703–712.
- 556 20. Li Jing, Zongcai Feng, Gerard Schuster, Wave-equation dispersion inversion, *Geophysical Journal*
557 *International*, Volume 208, Issue 3, 1 March 2017, Pages 1567–1578.
- 558 21. Lorenzo, J.M., Goff, D.S., Hayashi, K. "Soil-Type estimation beneath a coastal protection levee, using
559 resistivity and shear wave velocity" 22nd European Meeting of Environmental and Engineering
560 Geophysics, Near Surface Geoscience 2016.
- 561 22. Lutz K., Fechner T., Schevenels M., Stijn F. and Degrande G., 2011, Geotechnical characterization of a
562 river dyke by surface waves, *Near Surface Geophysics*, Volume9, Issue6, Pages 515-527.
- 563 23. Min D.-J. and Kim H.-S. 2006. Feasibility of the surface-wave method for the assessment of physical
564 properties of a dam using numerical analysis. *Journal of Applied Geophysics* 59, 236–243.
- 565 24. Pageot, D., Le Feuvre, M., Donatienne, L., Philippe, C., Yann, C., 2016. Importance of a 3D forward
566 modeling tool for surface wave analysis methods, in: EGU General Assembly Conference Abstracts. p.
567 11812.
- 568 25. Pan Yudi, Lingli Gao, Renat Shigapov, Multi-objective waveform inversion of shallow seismic
569 wavefields, *Geophysical Journal International*, Volume 220, Issue 3, March 2020, Pages 1619–1631.
- 570 26. Park, C. B., Xia, J., and Miller, R. D., 1998, Imaging dispersion curves of surface waves on
571 multichannel record: 68th Ann. Internat. Mtg., Soc. Explor. Geophys., Expanded Abstracts, 1377-1380.
- 572 27. Rahimi S., Clinton M. Wood, Folaseye Coker, Timothy Moody, Michelle Bernhardt-Barry, Behdad
573 Mofarraj Kouchaki, 2018, The combined use of MASW and resistivity surveys for levee assessment: A
574 case study of the Melvin Price Reach of the Wood River Levee, *Engineering Geology*, Volume 241,
575 Pages 11-24.
- 576 28. Samui, P., Sitharam, T.G. Correlation between SPT, CPT and MASW (2010) *International Journal of*
577 *Geotechnical Engineering*, 4 (2), pp. 279-288.
- 578 29. Samyn, K., Mathieu, F., Bitri, A., Nachbaur, A., Closset, L., 2014. Integrated geophysical approach in
579 assessing karst presence and sinkhole susceptibility along flood-protection dykes of the Loire River,
580 Orléans, France. *Eng. Geol.* 183, 170–184.
- 581 30. Sentenac P, Benes V, Keenan H (2018) Reservoir assessment using non- invasive geophysical
582 techniques. *Environmental Earth Sciences* 77(293):1-14
- 583 31. Socco, L.V. and Boiero, D., 2008. Improved Monte Carlo inversion of surface wave data, *Geophys.*
584 *Prospect.*, 56, 357–371.
- 585 32. Socco, L. V., D. Boiero, S. Foti, and R. Wisén, 2009, Laterally constrained inversion of ground roll
586 from seismic reflection records: *Geophysics*, 74, no. 6, G35–G45.
- 587 33. Socco, L. V., and C. Comina, 2015, Approximate direct estimate of S-wave velocity model from surface
588 wave dispersion curves: 21st Annual International Conference and Exhibition, EAGE, Extended
589 Abstracts, A09.
- 590 34. Socco, L.V., Comina, C. and Khosro Anjom, F., 2017. Time-average velocity estimation through
591 surface-wave analysis: Part 1—S-wave velocity, *Geophysics*, 82(3), U49–U59.
- 592 35. Socco, L.V. and Comina, C., 2017. Time-average velocity estimation through surface-wave analysis:
593 Part 2—P-wave velocity, *Geophysics*, 82(3), U61–U73.
- 594 36. Takahashi T, Yamamoto T (2010) An attempt at soil profiling on a river embankment using geophysical
595 data. *Explor Geophys* 41(1):102–108
- 596 37. Takahashi, T., Aizawa, T., Murata, K., Nishio, H., Mat-suoka, T. "Soil permeability profiling on a river
597 embankment using integrated geophysical data", 2014, SEG Technical Program Expanded Abstracts,
598 33, pp. 4534-4538.
- 599 38. Teodor D., Comina C., Khosro Anjom F., Socco L.V., Brossier R. and Virieux J., 2020, Challenges in
600 shallow targets reconstruction by 3D elastic full-waveform inversion – Which initial model?, submitted
601 to *Geophysics*.



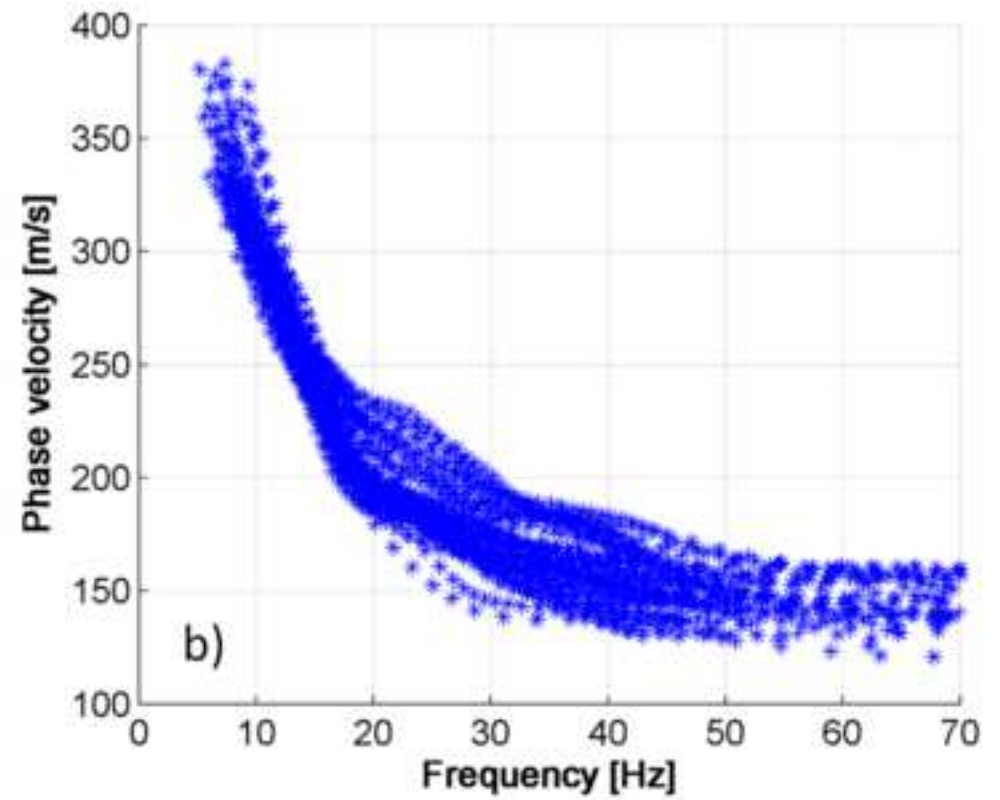
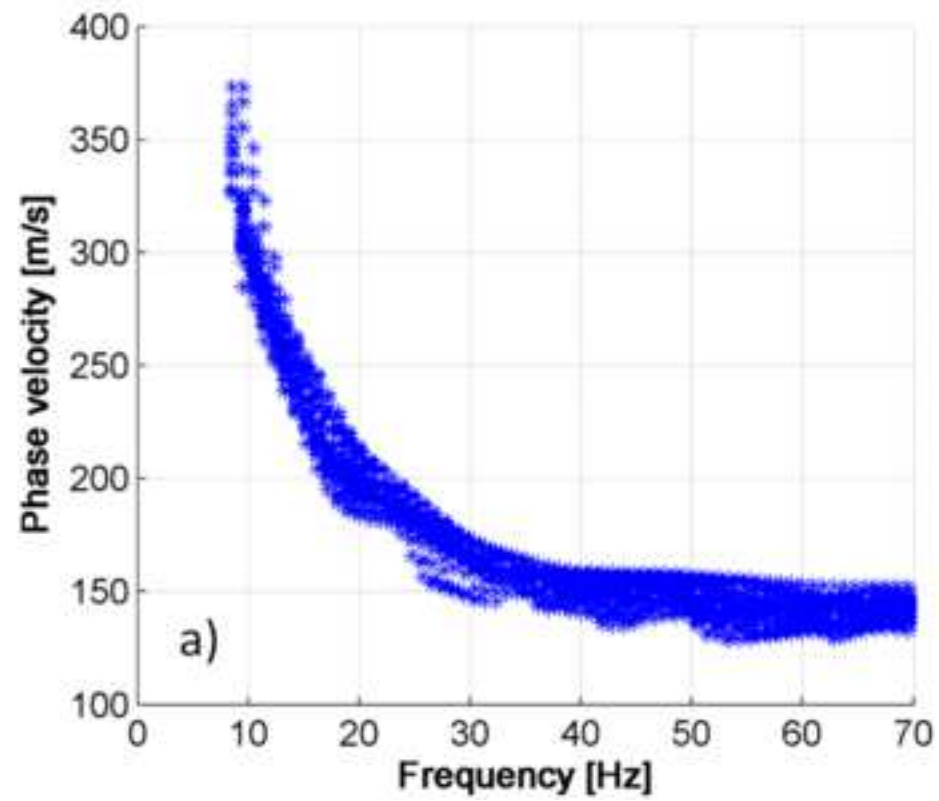


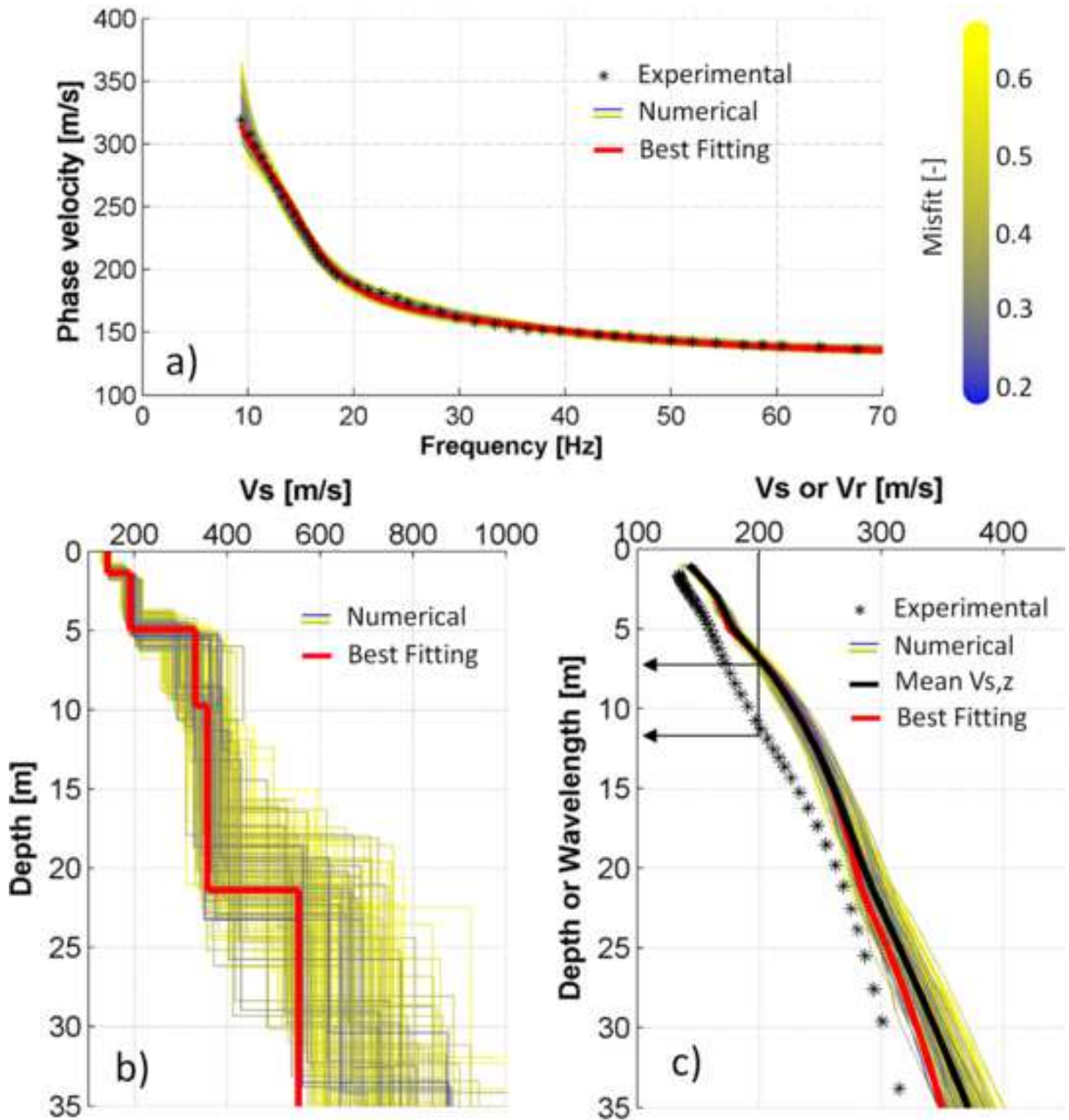


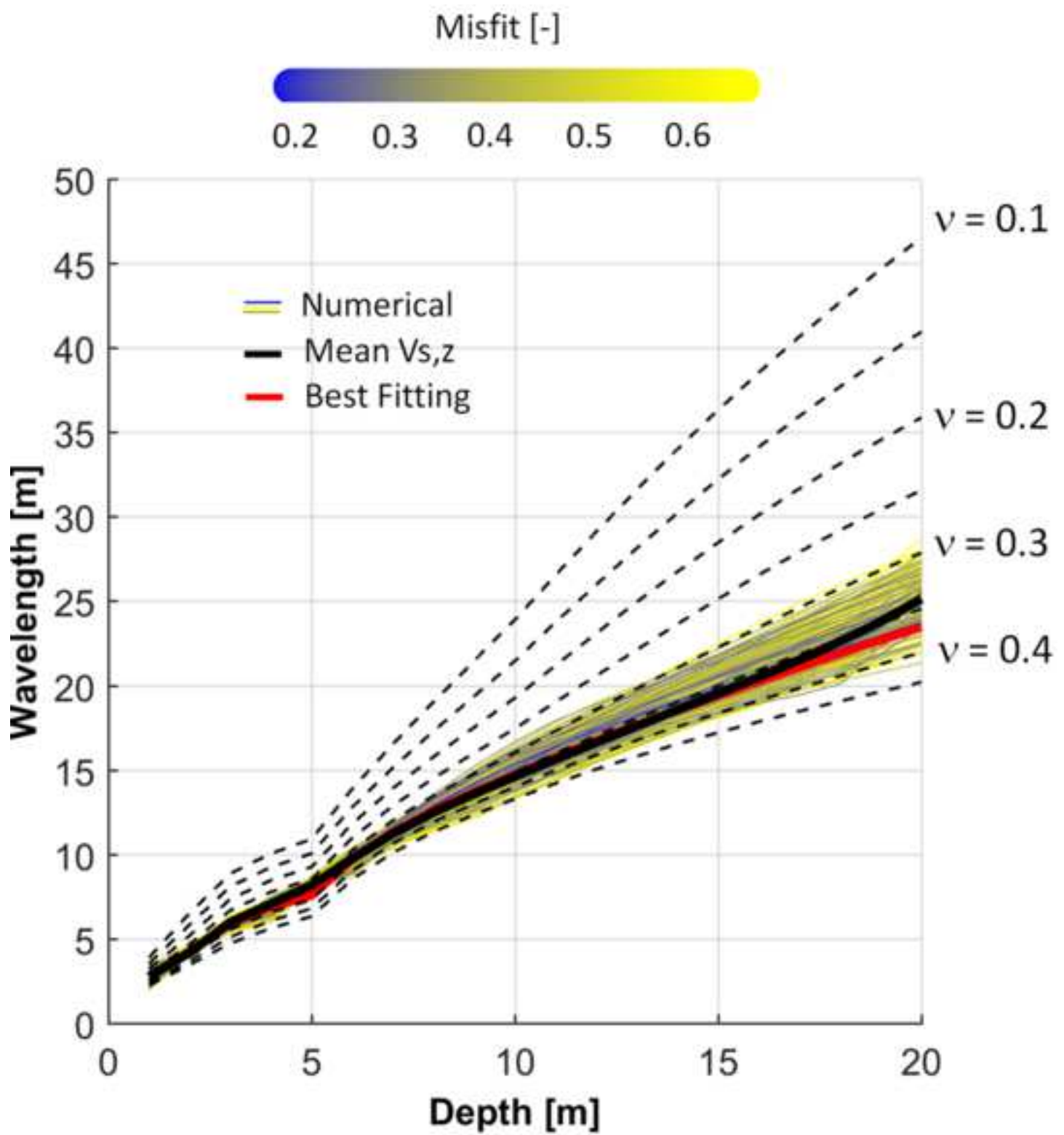
a)

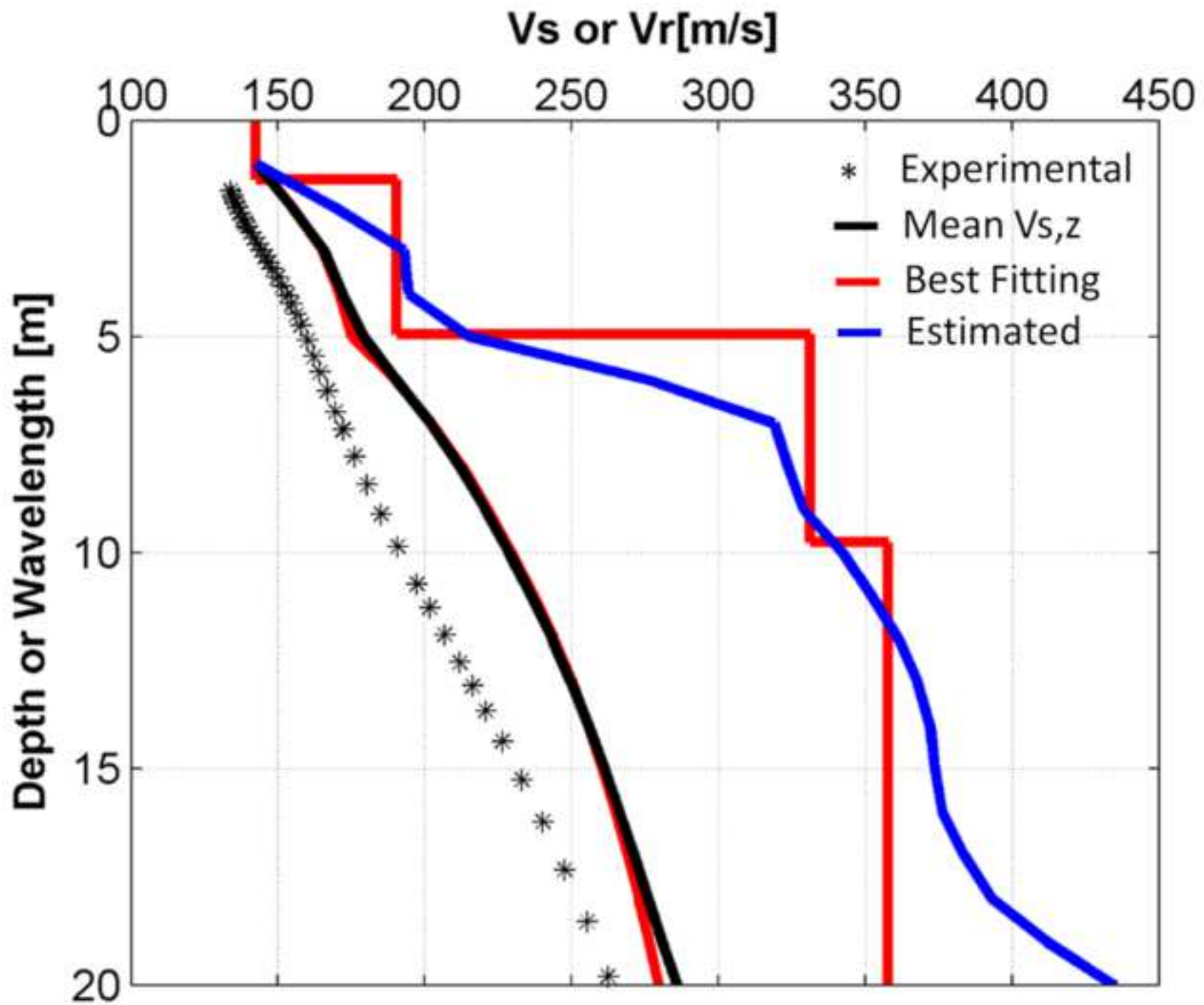


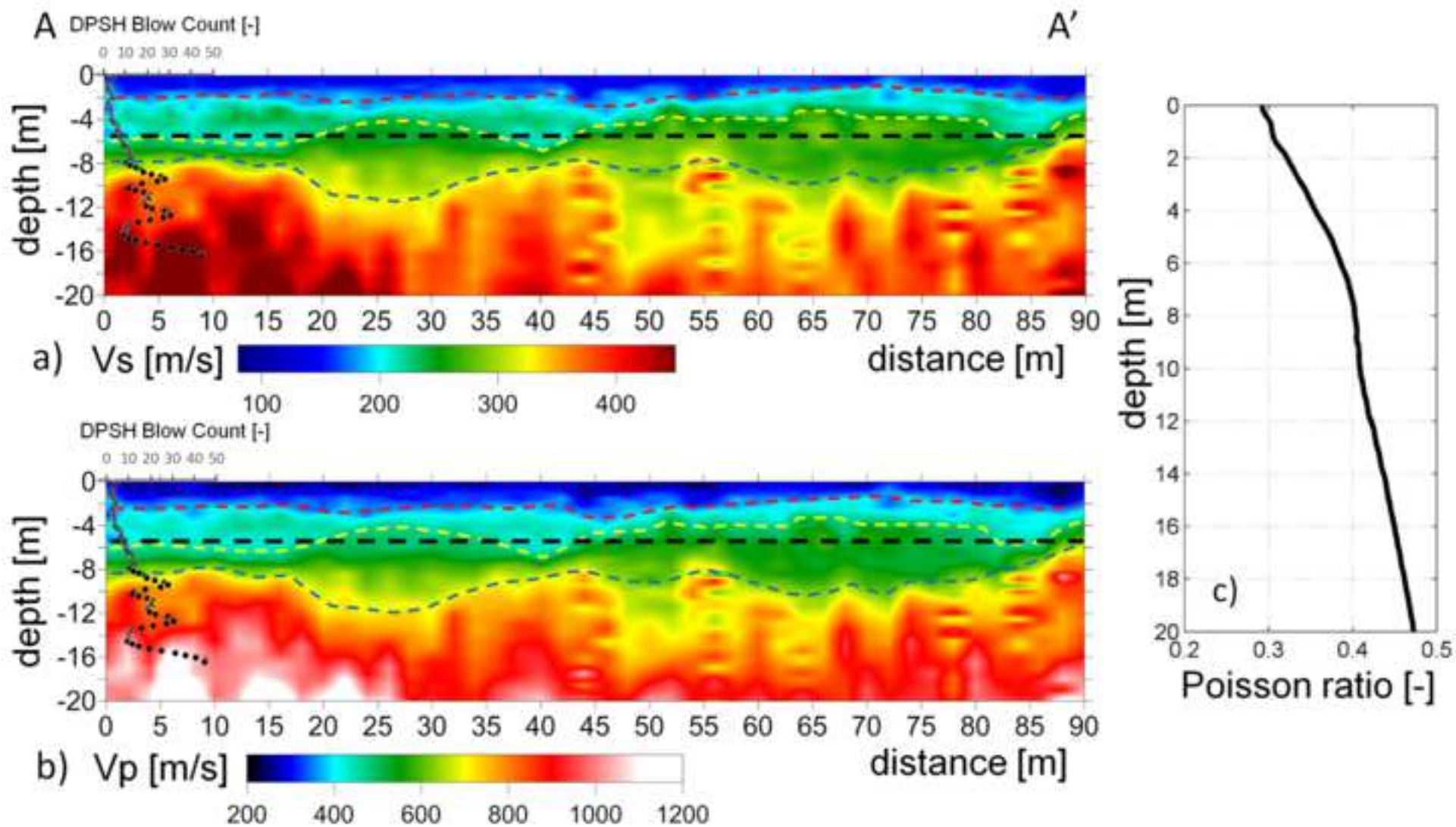
b)

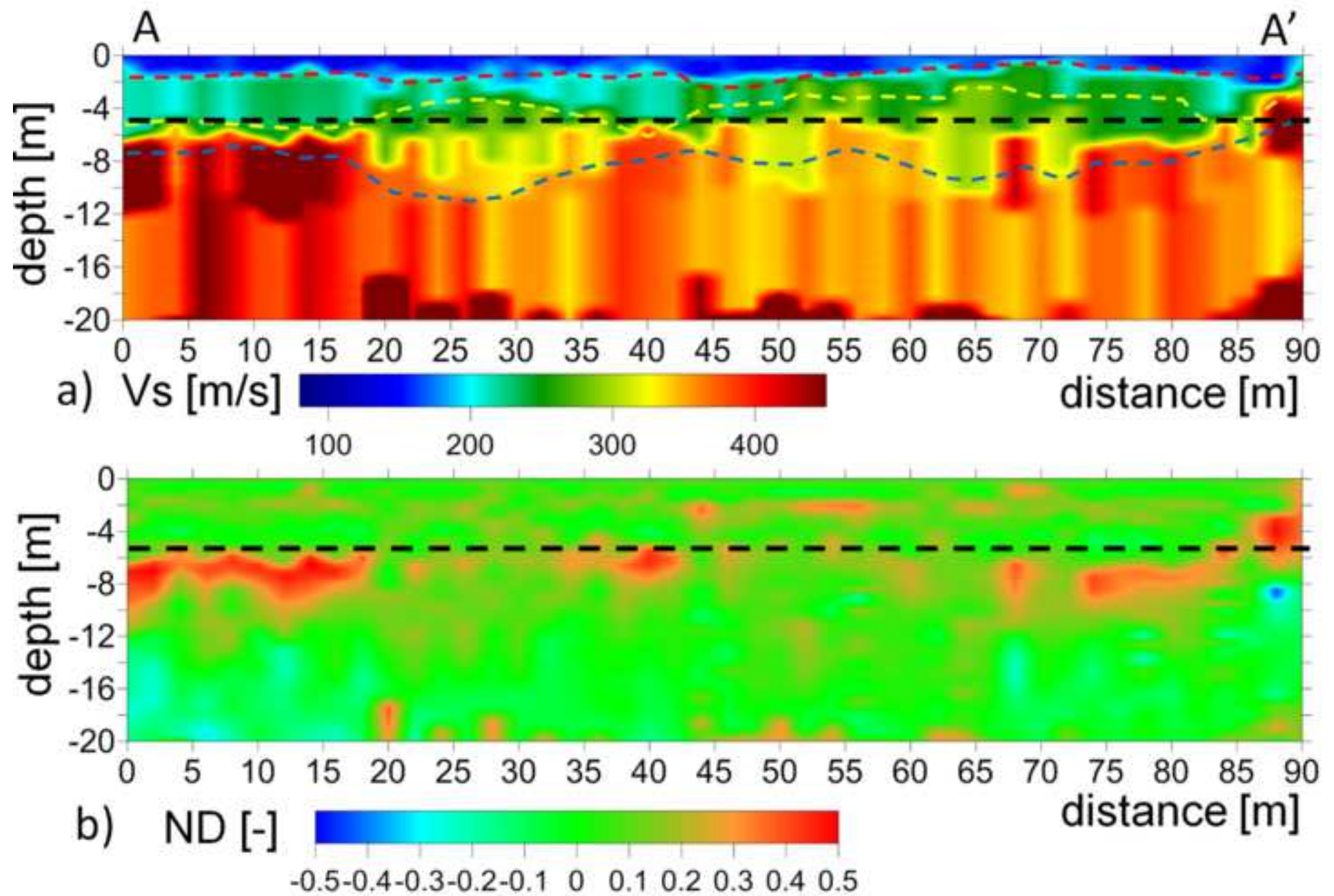


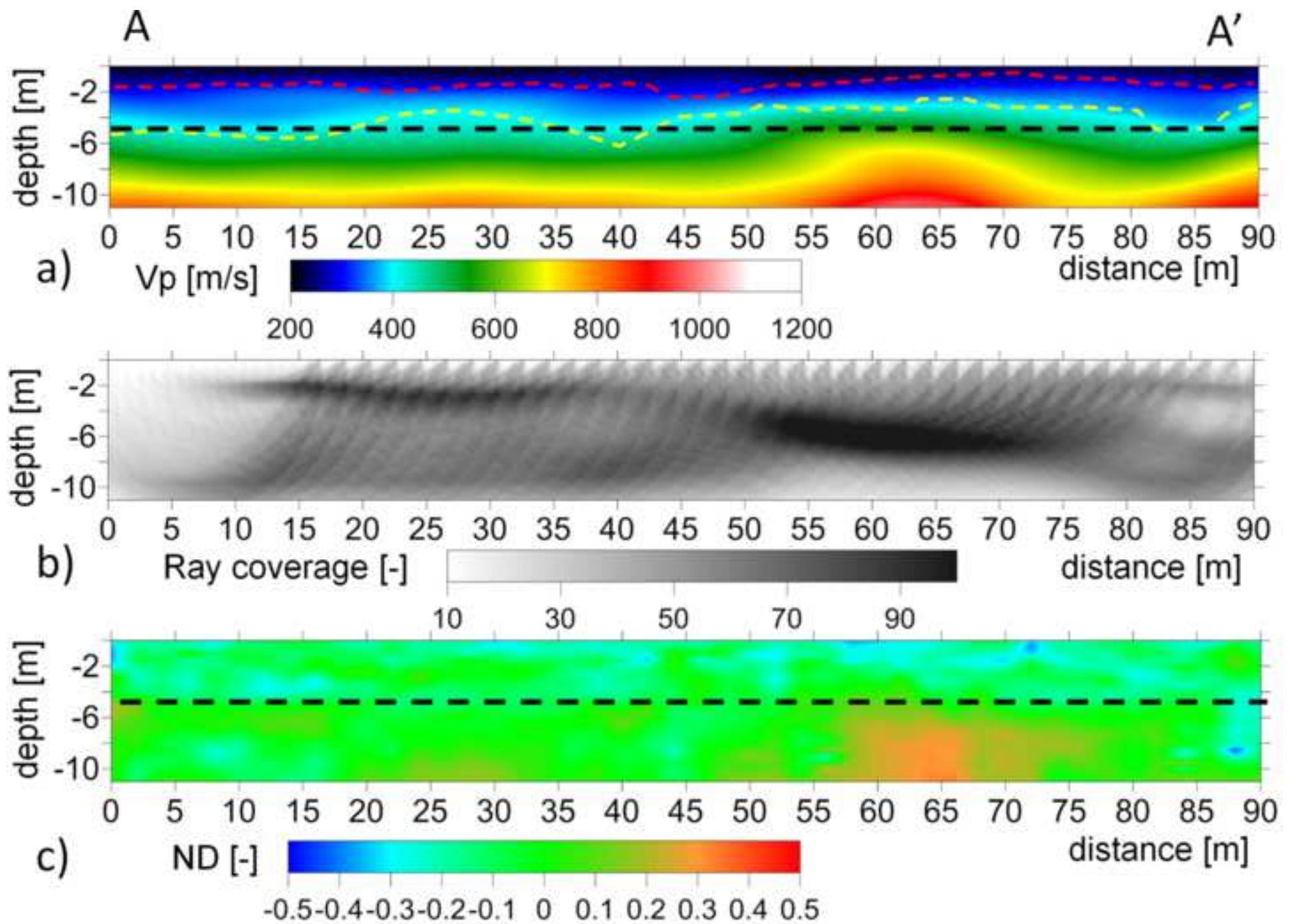


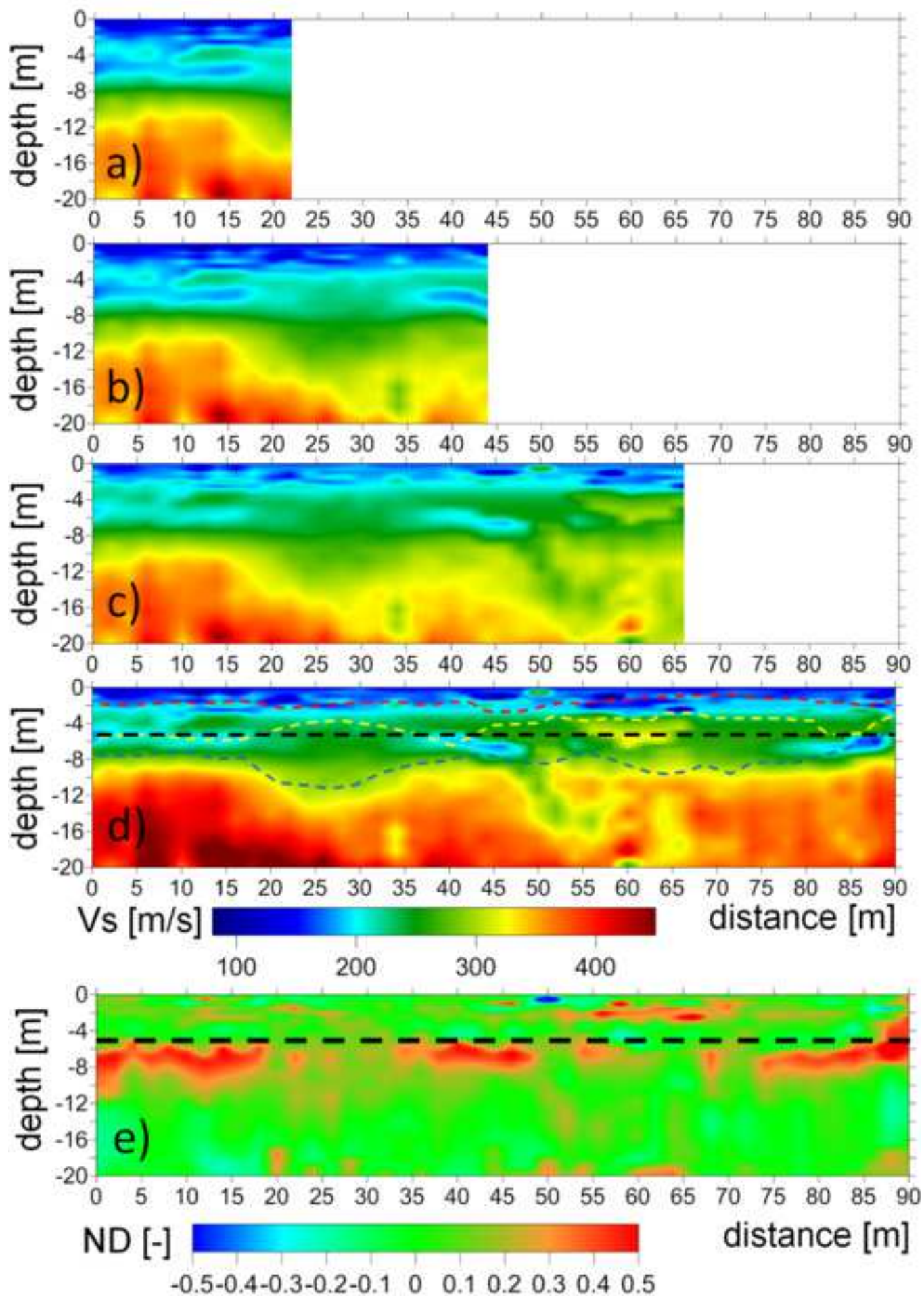


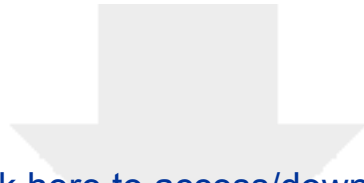












Click here to access/download
RDM Data Profile XML
DataProfile_5454589.xml



Declaration of interests

The authors declare that they have no known competing financial interests or personal relationships that could have appeared to influence the work reported in this paper.

The authors declare the following financial interests/personal relationships which may be considered as potential competing interests:

Title: **Effective V_s and V_p characterization from Surface Waves streamer data along river embankments.**

Authors: **Comina C.** Writing - Original Draft, Conceptualization, Methodology, Investigation, Data Curation, Visualization

Vagnon F. Writing - Review & Editing, Conceptualization, Investigation, Data Curation, Visualization

Arato A. Writing - Review & Editing, Conceptualization, Methodology, Investigation, Project administration, Funding Acquisition

Antonietti A. Data Curation, Investigation